

**UNCLASSIFIED**

---

**AD 296 513**

*Reproduced  
by the*

**ARMED SERVICES TECHNICAL INFORMATION AGENCY  
ARLINGTON HALL STATION  
ARLINGTON 12, VIRGINIA**



---

**UNCLASSIFIED**

**NOTICE:** When government or other drawings, specifications or other data are used for any purpose other than in connection with a definitely related government procurement operation, the U. S. Government thereby incurs no responsibility, nor any obligation whatsoever; and the fact that the Government may have formulated, furnished, or in any way supplied the said drawings, specifications, or other data is not to be regarded by implication or otherwise as in any manner licensing the holder or any other person or corporation, or conveying any rights or permission to manufacture, use or sell any patented invention that may in any way be related thereto.

63-2-4

TR-1073

29 6513

296 513

## FLUID AMPLIFICATION

CATALOGUE BY ADTIA

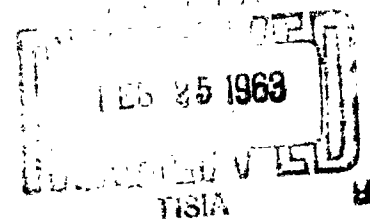
AS AD NO.

### 1. Gain Analysis of the Proportional Fluid Amplifier

S. J. Peperone

Silas Katz

John M. Goto



30 October 1962



**DIAMOND ORDNANCE FUZE LABORATORIES**  
**ORDNANCE CORPS • DEPARTMENT OF THE ARMY**

WASHINGTON 25, D. C.

## FLUID AMPLIFICATION

### 4. Gain Analysis of the Proportional Fluid Amplifier

#### ERRATA SHEET

Page 13. Under Section 3. Analysis of Power-Jet Deflection, the first assumption should read:

1) The fluid is incompressible

Page 17. Equation 4 should be:

$$dQ_o = \frac{\partial Q_o}{\partial \theta} d\theta + \frac{\partial Q_o}{\partial \theta_s} d\theta_s + \frac{\partial Q_o}{\partial \theta_d} d\theta_d + \frac{\partial Q_o}{\partial l} dl$$

Page 17. Equation 6 should be:

$$G_Q = \frac{\partial Q_o}{\partial \theta_s} \frac{d\theta_s}{dQ_1}$$

Page 17. Equation 7a should be:

$$v_{av} = \left( \sqrt{\frac{2g_c}{\rho}} \right) \left( \frac{1}{\theta_d} \int_0^{\theta_d} p^{\frac{1}{2}} (\theta + \theta_s, l) d\theta \right)$$

Page 19. In the paragraph below equation 15, L should be l

Page 22. Line 1 should read:  
When these values,.....equation 11, 21

Page 28. Abscissa on figure 11 should be:  
 $\theta_d$ , (standard deviation  $\sigma$ )

**DIAMOND ORDNANCE FUZE LABORATORIES**  
**ORDNANCE CORPS**                      **WASHINGTON 25, D. C.**

DA-5N03-01-003

TR-1073

OMS Code 5010.11.71200

DOFL Proj 31100

30 October 1962

**FLUID AMPLIFICATION**

**4. Gain Analysis of the Proportional Fluid Amplifier**

**S. J. Peperone**

**Silas Katz**

**John M. Goto**

**FOR THE COMMANDER:**  
**Approved by**

*R. D. Hatcher*  
R. D. Hatcher  
Chief, Laboratory 300



Qualified requesters may obtain copies of this report from ASTIA.

## FOREWORD

This publication is the fourth in a DOFL-report series on the basic design and operating principles of fluid amplification. As reported in reference 1, the objective of a proportional fluid amplifier is to achieve—without mechanical moving parts—the control of fluid power by a lesser amount of power. A realization of this objective, which was proved feasible, would result in a fluid device having signal-power gain, small-signal linearity, broad bandwidth, and high reliability. In many respects, the device would be analogous to the transistor in the field of electronics.

Specifically, this report presents a theoretical analysis of pressure, volume flow, and power gains of a proportional fluid amplifier and compares predictions with experimental data. The analysis was made assuming an incompressible fluid; the measurements were made using air at pressures less than 5 psig.

Also included are generalized background discussions on jet-stream characteristics and power-jet deflections.

# NOMENCLATURE

$A$ = area	$\text{ft}^2$
$b$ = output aperture width	$\text{ft}$
$F$ = force	$\text{lbf}$
$G$ = gain	nondimensional
$g_c$ = conversion factor	$\frac{32.2 \text{ lbm ft}}{\text{lbf sec}^2}$
$L$ = distance from point of apparent emanation of the power jet to output apertures	$\text{ft}$
$l$ = distance from power nozzle exit to output aperture	$\text{ft}$
$p$ = total pressure (gauge)	$\text{lbf/ft}^2$
$Q$ = volume flow rate	$\text{ft}^3/\text{sec}$
$v$ = velocity	$\text{ft/sec}$
$w$ = nozzle width	$\text{ft}$
$\alpha$ = ratio of dynamic to total pressure (gauge)	nondimensional
$\gamma$ = stream deflection angle (measured from interaction region)	radians (or deg)
$\theta$ = angle to arbitrary point of stream	radians (or deg)
$\theta_s$ = stream deflection angle	radians (or deg)
$\rho$ = density	$\text{lbm/ft}^3$
$\sigma$ = standard deviation	radians (or deg)
$\phi$ = angle of spread of the power stream	radians (or deg)
$\theta_d$ = angle subtended by one output aperture	radians (or deg)

NOMENCLATURE—Continued  
(Subscripts)

1 = power stream  
2 = left-control stream  
3 = right-control stream  
av = average value  
d = output aperture  
i = signal input  
L = left-output aperture entrance  
m = maximum value  
o = signal output  
p = pressure  
pQ = power  
Q = flow rate  
R = right-output aperture entrance  
s = static conditions

## CONTENTS

	Page
FOREWORD . . . . .	3
NOMENCLATURE . . . . .	5
LIST OF ILLUSTRATIONS . . . . .	8
1. INTRODUCTION . . . . .	9
2. CHARACTERISTICS OF JET STREAMS . . . . .	9
3. ANALYSIS OF POWER-JET DEFLECTION . . . . .	13
4. THEORETICAL DEVELOPMENT OF GAIN . . . . .	14
4.1 Flow Gain . . . . .	14
4.2 Pressure Gain . . . . .	19
4.3 Power Gain . . . . .	20
5. APPLICATION OF THEORY . . . . .	21
5.1 Predicting the Gain of a Fluid Amplifier . . . . .	21
5.2 Optimization of Gain. . . . .	22
5.2.1 Constant-Width Apertures . . . . .	22
5.2.2 Constant-Deviation Apertures . . . . .	22
5.2.3 Varying-Width Apertures. . . . .	22
6. TEST SETUP AND PROCEDURE . . . . .	29
7. COMPARISON OF THEORETICAL AND EXPERIMENTAL RESULTS . . . . .	29
7.1 Flow Difference . . . . .	32
7.2 Pressure Difference . . . . .	32
8. DISCUSSION . . . . .	32
9. CONCLUSIONS. . . . .	37
10. REFERENCES . . . . .	38
APPENDIX A: THEORETICAL ANALYSIS OF INTERACTING STREAMS—MATH- MATICAL DERIVATIONS . . . . .	39

## ILLUSTRATIONS

### Figure

- 1 Proportional fluid amplifier—basic design.
- 2 Power-jet pressure profile at entrance to output apertures.
- 3 Schematic diagram of jet diffusion.
- 4 Experimental profiles.
- 5(a) Jet impinging on a flat wall.
- 5(b) Fluid amplifier interaction region.
- 6 Theoretical flow gain versus stream deflection with stream width as a parameter.
- 7 Theoretical pressure gain versus stream deflection with stream width as a parameter.
- 8 Theoretical power gain versus stream deflection with stream width as a parameter.
- 9 Theoretical gain versus downstream distance constant-width aperture ( $\theta_s = 0$ ).
- 10 Theoretical gain versus downstream distance constant-deviation apertures ( $\theta_s = 0$ ).
- 11 Theoretical gain versus aperture width fixed distance downstream ( $\theta_s = 0$ ).
- 12 Proportional amplifier.
- 13 Functional diagram of test setup.
- 14,15 Comparison of experimental and theoretical flow differences.
- 16,17 Comparison of experimental and theoretical pressure differences.
- A1 Free body diagrams of the interacting streams.

## 1. INTRODUCTION

To achieve fluid amplification without mechanical moving parts, a power nozzle is used to transform the energy initially stored in static pressure into dynamic pressure. This power stream of high energy fluid passes through an interaction region and is partitioned into two output apertures as shown in figure 1. Control streams placed at each side and usually normal to the power stream determine the direction of flow of the power stream. Variations in the net thrust of the control streams change the deflection of the power stream, and thereby change the division of fluid between the two output apertures (fig. 2).

The gain of a proportional amplifier is defined as the ratio of the change in the variable of interest at the output to the change of this variable at the input—that is, the ratio of output to input signal. The theoretical analysis that follows was made of the gains in pressure, volume flow, and power; predictions were compared with experimental data. An incompressible fluid was assumed in this analysis and the measurements were made using air at less than 5 psig.

## 2. CHARACTERISTICS OF JET STREAMS

The operation of a proportioning fluid amplifier is dependent upon controlling and collecting the fluid stream issuing from a nozzle. To understand fluid amplification, therefore, some knowledge of jet-stream characteristics is necessary.

A fluid stream discharging into a fluid initially at rest undergoes both lateral diffusion and deceleration (ref 2) while the surrounding fluid is brought into motion. The reason for this is that, at the exit of the nozzle, a high velocity gradient exists between the stream and the surrounding fluid. Eddies generated in this region produce a lateral mixing process resulting in the formation of two distinct regimes (fig. 3), the zone of establishment and the zone of established flow. Over an extremely wide range of Reynolds number (ref 2), the stream characteristics remain essentially unchanged. The zone of establishment ends about 6 nozzle widths downstream from the nozzle exit for the conditions of interest here. In this zone the mixing process has not penetrated to the center line of the jet stream, and the conditions at the center line are still the same as at the nozzle exit. At approximately 6 nozzle widths the fluid enters the zone of established flow. In this region the velocity throughout the stream decreases as the distance from the nozzle exit increases.

The fluid in the amplifier under consideration differs from the stream described above, because it is confined between parallel

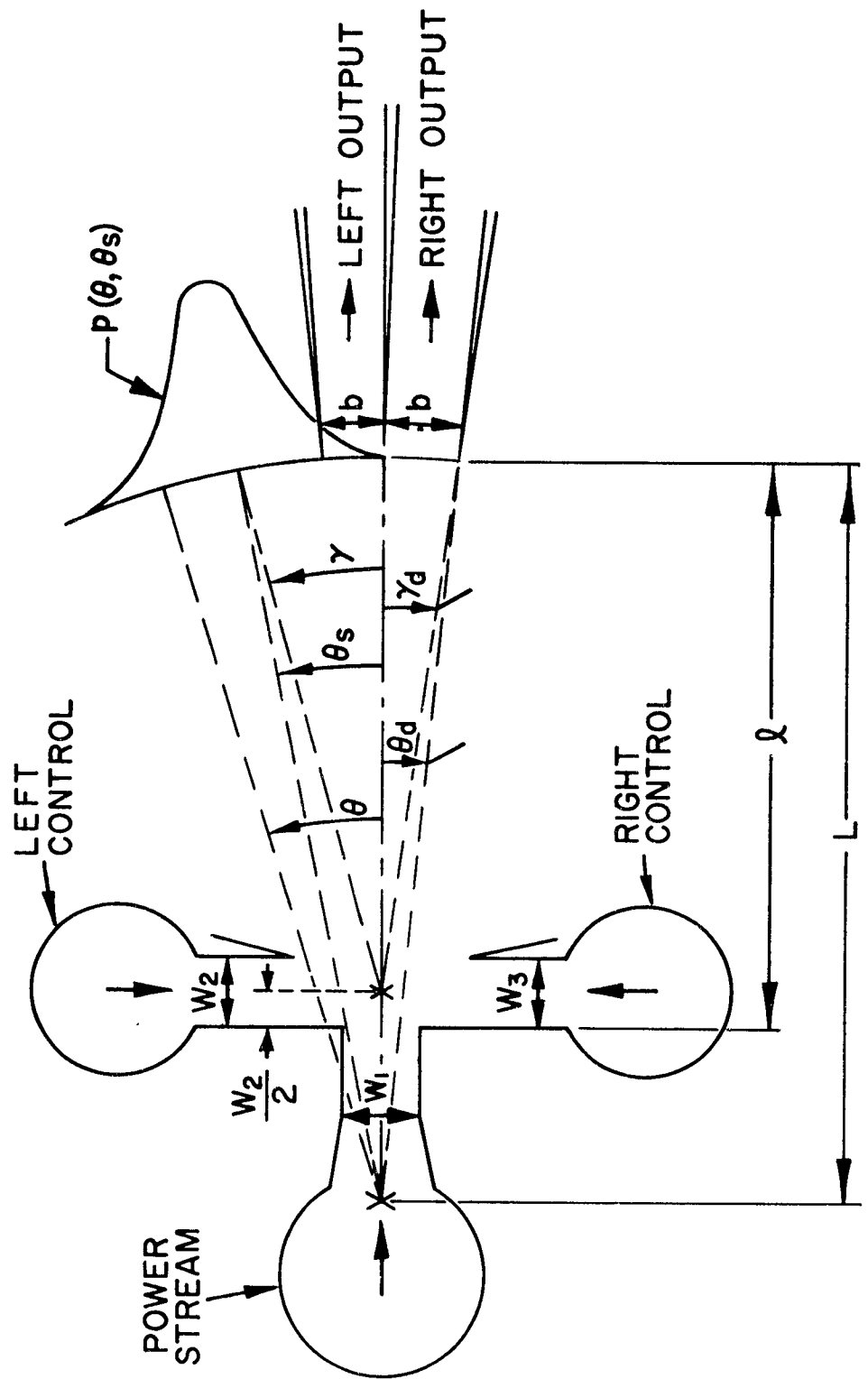


Figure 1. Proportional fluid amplifier—basic design.

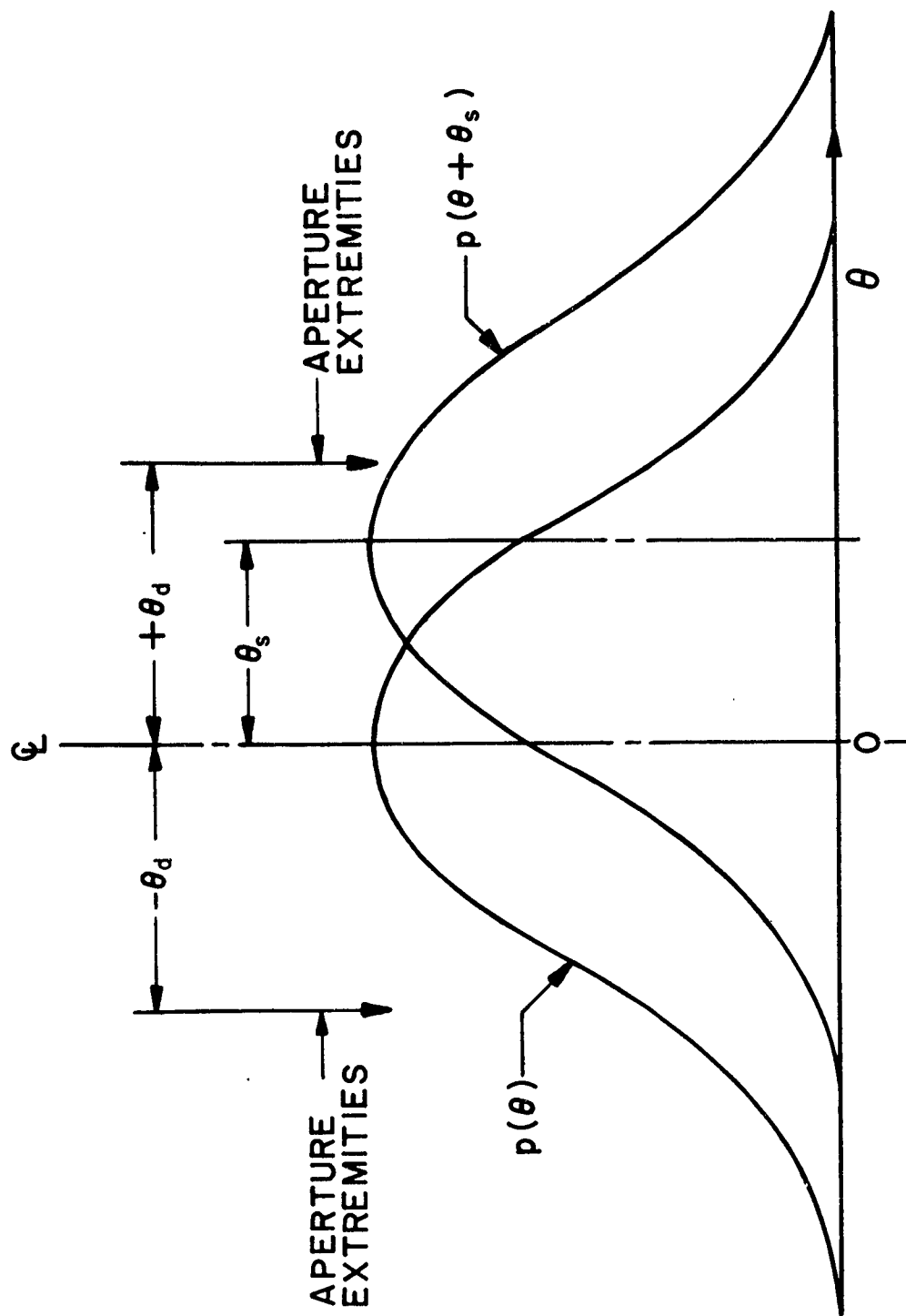


Figure 2. Power-jet pressure profile at entrance to output apertures.

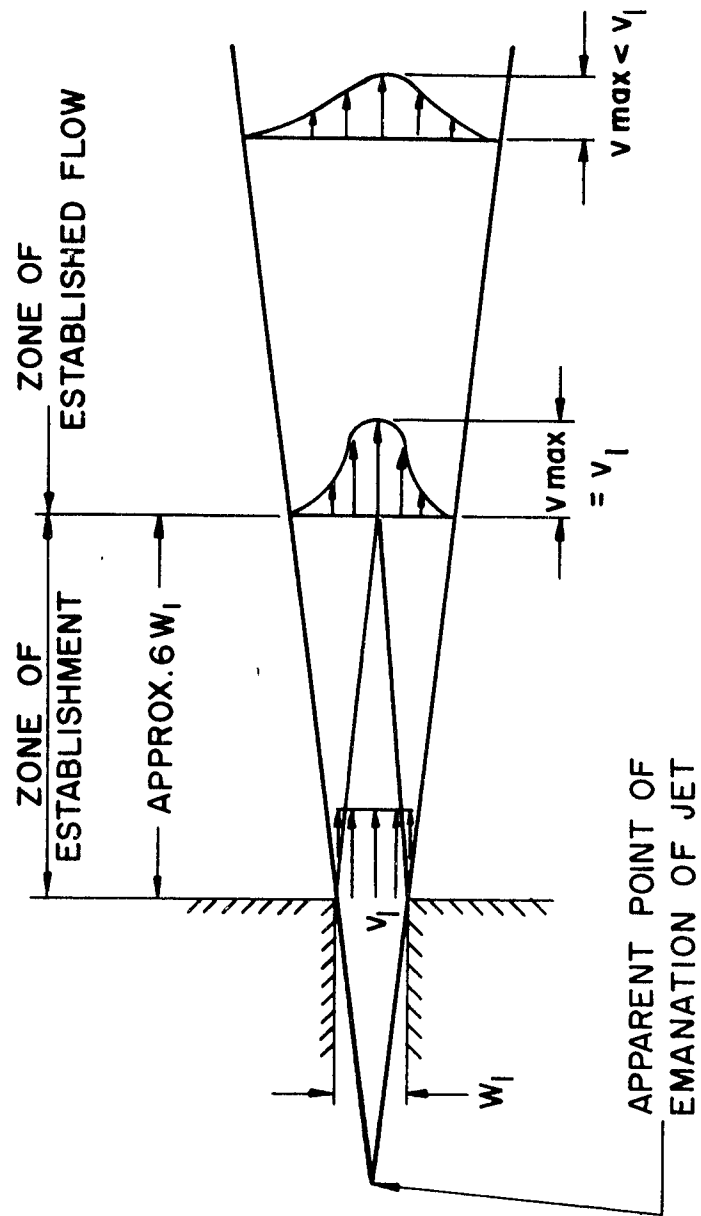


Figure 3. Schematic diagram of jet diffusion.

plates. In the unconfined stream, only the tangential shear within the mixing region decelerates the jet stream, and since this process is completely internal, momentum flux is conserved. In the confined stream, the top and bottom plates exert a shearing force on the stream. This process is external to the stream, and momentum flux is not conserved. Consequently, the zone of established flow appears to emanate from a point on the center line farther upstream from the nozzle than the apparent point of emanation of an unconfined stream (ref 3).

Dynamic pressure profiles (taken at DOFL) of a two-dimensional (2-D) stream confined between parallel plates are shown in figure 4. The ratio of the distance between plates to the nozzle width (aspect ratio) was 8. Integration of these profiles confirms the fact that momentum flux is not conserved, but decreases with increasing distance from the nozzle exit. In this case, the stream appears to emanate from a point 4 nozzle widths upstream from the exit. As the aspect ratio is lowered this distance is expected to increase.

The maximum pressure of these experimental profiles occurs on the center line of the stream. These data show that the maximum pressure 7 nozzle widths downstream of the exit dropped to 95 percent of the exit pressure; at 11 nozzle widths, to 68 percent of the exit pressure. The shape of these profiles is similar to those found in reference 2 for 2-D jets without parallel plates.

It is to be noted that the experimental profiles were obtained in the absence of output apertures. Experimental evidence indicates that the static pressure throughout the zones of motion is constant if no obstructions are present. The stagnation pressure at the edges of the apertures affects the profiles; however, if the edges are sharp, this effect is believed to be small.

### 3. ANALYSIS OF POWER-JET DEFLECTION

The following analysis of the power-jet deflection by means of the control stream is based on three assumptions:

- (1) The fluid is incompressible and steady.
- (2) The flow is steady.
- (3) The impingement of the control stream on the power stream may be viewed as a 2-D potential motion problem where the power jet is considered as a nondeformable wall. This means that there is no mixing between the control and power streams.

The thrust exerted by the control stream on the power jet is computed from Newton's second law, which for a frictionless fluid in steady motion may be written as

$$\sum \vec{F} = \oint_{\text{surface}} \frac{\rho}{g_c} (\vec{v} \cdot d\vec{A}) \vec{v} + \oint_{\text{surface}} p_s d\vec{A} \quad (1)$$

where  $\rho$  and  $\vec{v}$  are the density and velocity of the control stream,  $d\vec{A}$  is incremental area,  $p_s$  is static pressure, and  $g_c$  is the gravitational conversion factor. This equation simply states that the sum of the external forces acting on the system is equal to the rate of change of momentum of the bounded mass system.

Assuming that the problem of determining the velocity  $\vec{v}$  is similar to the classical problem of the impingement of an incompressible, frictionless, steady stream on a flat wall, the result is given by the curves of figure 5a.

The solution shows (ref 4) that the streamlines are hyperbolas whose asymptotes are the x and y axes. The control stream, therefore, follows along the side of the power jet with no bounce. If the configuration in figure 5a is modified by inserting walls at the middle and edge filaments, and if the power jet replaces the wall, the streamlines remain essentially unchanged (figure 5b).

The geometry of the classical problem now conforms to the interaction region of the fluid amplifier and  $\vec{v}$  is determined. The desired relation between stream thrust and deflection angle is derived in appendix A.

#### 4. THEORETICAL DEVELOPMENT OF GAIN

##### 4.1 Flow Gain

The flow gain  $G_Q$  of a proportional amplifier is defined as the ratio of the change in the output volumetric flow difference  $\Delta Q_o$  to the change in input volumetric flow difference  $\Delta Q_i$  so that

$$G_Q = \frac{\Delta Q_o}{\Delta Q_i} \quad (2)$$

or

$$G_Q = \frac{\Delta(Q_L - Q_R)}{\Delta(Q_2 - Q_3)} \quad (2a)$$

where the subscripts L and R refer to the left and right-output apertures, and 2 and 3 refer to the left and right-control nozzles, respectively.

The output-flow difference  $Q_o$  is a function of the pressure profile  $p(\theta, \theta_s)$ , the angle subtended by the apertures  $\theta_d$ , and the

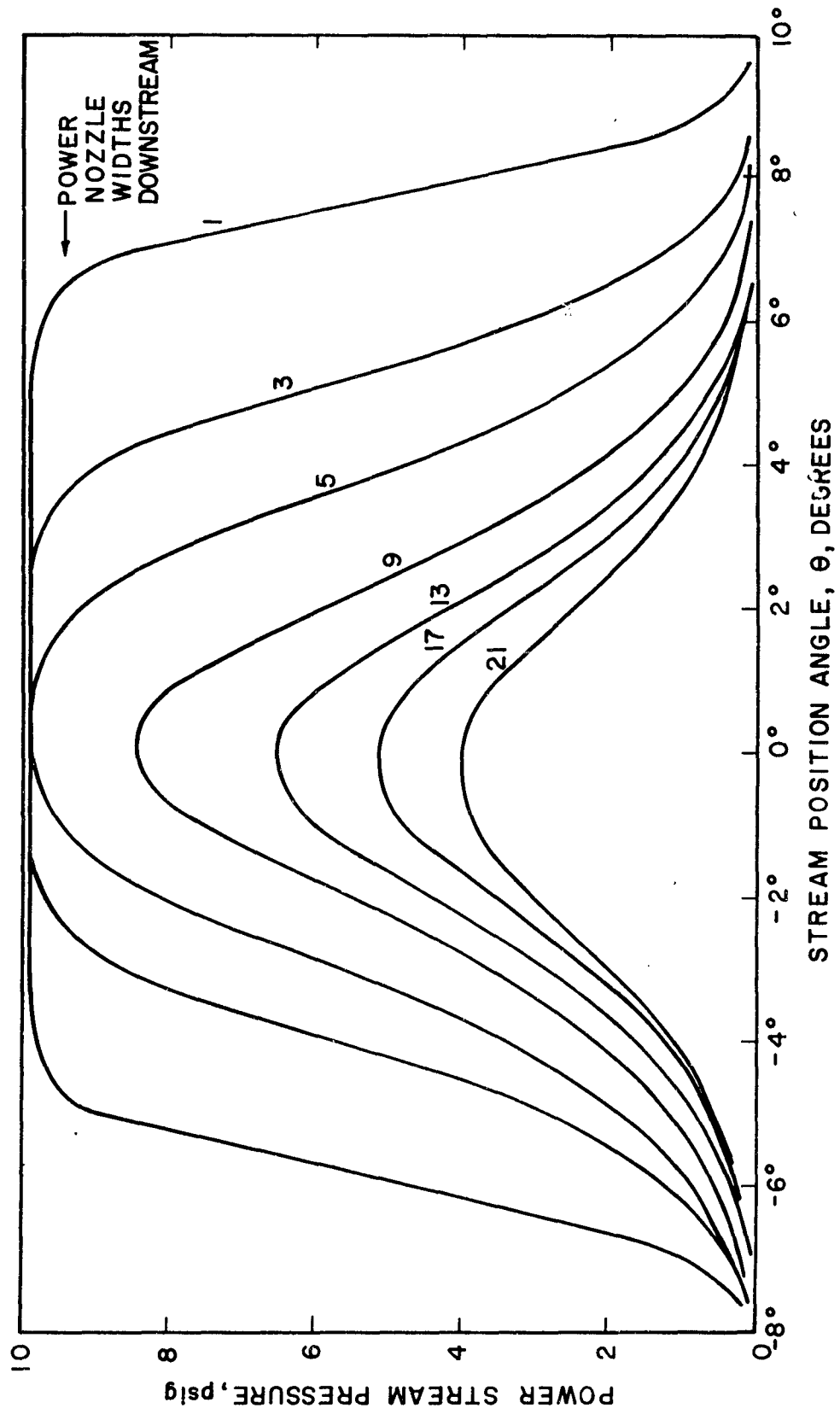


Figure 4. Experimental profiles.

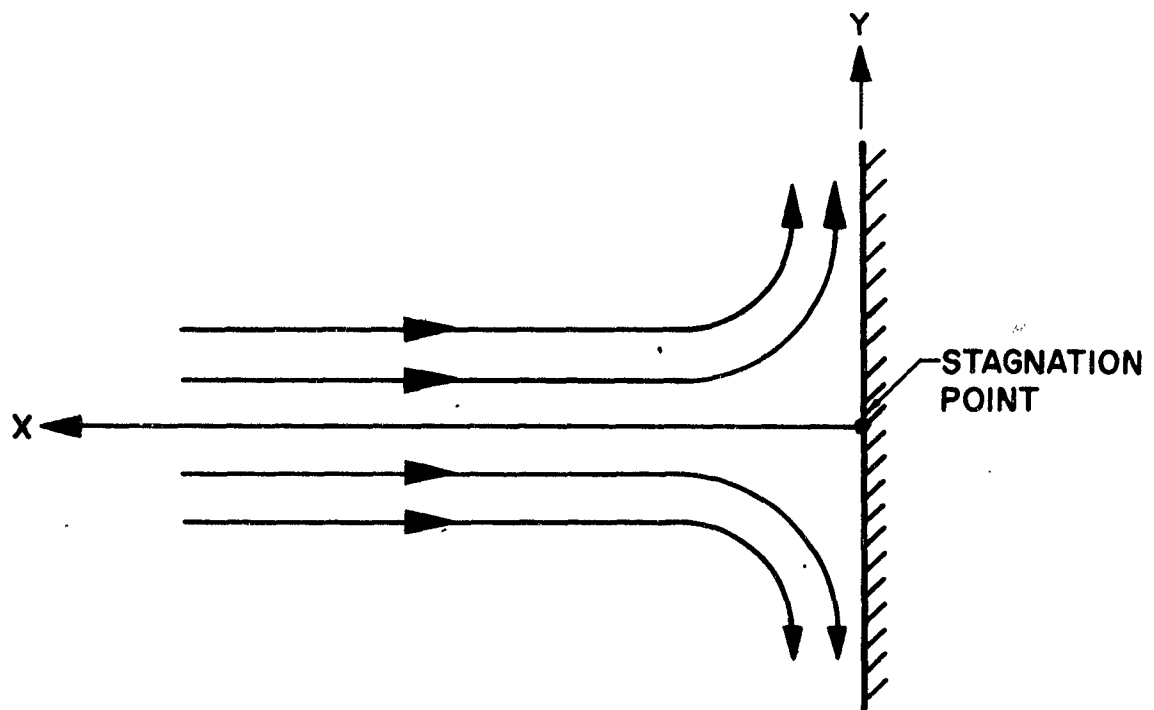


Figure 5(a). Jet impinging on a flat wall.

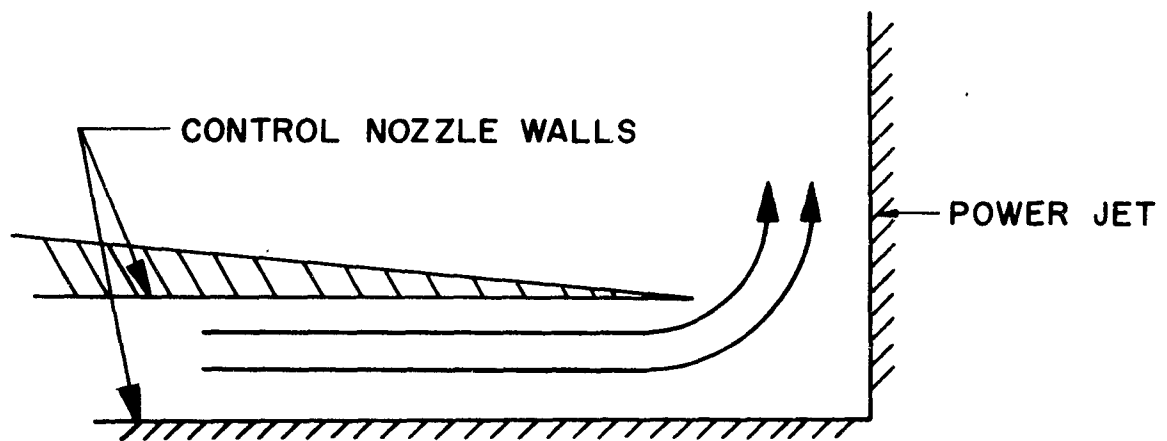


Figure 5(b). Fluid amplifier interaction region.

downstream distance of the apertures  $l$  (fig. 1), where  $\theta$  is an arbitrary angle and  $\theta_s$  is the stream deflection angle:

$$Q_o = Q_o(\theta, \theta_s, \theta_d, l) \quad (3)$$

The total differential of equation (3) is

$$dQ_o = \frac{\partial Q_o}{\partial \theta} d\theta + \frac{\partial Q_o}{\partial \theta_s} d\theta_s + \frac{\partial Q_o}{\partial \theta_d} d\theta_d + \frac{\partial Q_o}{\partial l} dl \quad (4)$$

For small increments, the flow gain may be written as

$$G_Q = \frac{dQ_o}{dQ_1} = \frac{\partial Q_o}{\partial \theta} \frac{d\theta}{dQ_1} + \frac{\partial Q_o}{\partial \theta_s} \frac{d\theta_s}{dQ_1} + \frac{\partial Q_o}{\partial \theta_d} \frac{d\theta_d}{dQ_1} + \frac{\partial Q_o}{\partial l} \frac{dl}{dQ_1} \quad (5)$$

Assuming that the pressure profile does not change for small control inputs,  $\frac{d\theta}{dQ_1} = 0$ ; and since  $\theta_d$  and  $l$  are independent of  $Q_1$ , the gain expression reduces to

$$G_Q = \frac{\partial Q_o}{\partial \theta_s} \frac{d\theta_s}{dQ_1} \quad (6)$$

From the definition of flow rate, the output flow difference may be written as

$$Q_o = A_L v_{avL} - A_R v_{avR} \quad (7)$$

where  $A_L$ , for example, is the area of the left aperture and  $v_{av}$  is the average velocity. For an incompressible fluid, the total pressure at the entrances and exits of the apertures is the sum of the static and dynamic pressure; moreover, the static pressure of the fluid stream approaching nonloaded apertures is ambient, so that the output volume flow rate may be computed from  $p = \frac{\rho}{2g_c} v^2$ .

In terms of the pressure profile  $p(\theta + \theta_s, l)$  the average velocity is

$$v_{av} = \sqrt{\frac{2g_c}{\rho}} - \frac{1}{\theta_d} \int_{-\theta_d}^{\theta_d} p^{1/2}(\theta + \theta_s, l) d\theta \quad (7a)$$

and the output volume flow rate is

$$Q_o = \frac{1}{\theta_d} \sqrt{\frac{2g_c}{p}} \left[ A_L \int_0^{\theta_d} p^{1/2} (\theta + \theta_s, l) d\theta - A_R \int_{-\theta_d}^0 p^{1/2} (\theta + \theta_s, l) d\theta \right] \quad (8)$$

The relation between stream deflection  $\gamma$  and input-flow difference is derived (app A) by applying the momentum equation to the interaction region. If the left and right control areas are equal, the relation is approximately

$$\tan \gamma = \frac{\rho(1+\alpha_2)(1+\sin \varphi)(Q_1^2 + 2Q_1 Q_3)}{2 g_c \alpha_2 A_1 A_2 (1+\alpha_1)(p_1)} \quad (9)$$

where  $\alpha$  is the ratio of dynamic to total pressure,  $\varphi$  is the difference in deflection between power stream and control stream, and the subscript 1 refers to the power nozzle.

It should be noted that the angles  $\theta_s$  and  $\gamma$  are measured from different vertices. Experiments have shown that the power stream appears to radiate from a source approximately 4 nozzle widths upstream of the power-jet exit (for an aspect ratio of 8), but it is deflected about the point of intersection of the power- and control-nozzle center lines.

From figure 1, the geometrical relation between angles  $\theta_s$  and  $\gamma$  is

$$\tan \theta_s = \frac{l - \frac{w_2}{2}}{L} \tan \gamma \quad (10)$$

where  $L$  is the downstream distance from the point of apparent emanation to the apertures and  $w_2$  is the control-nozzle width.

If the areas of the left and right apertures are equal, the theoretical flow gain obtained by combining eq (6), (8), (9), (10) and normalizing the pressure is

$$G_Q = \frac{K Q_2 A_1 A_d p_m^{1/2}(l)}{Q_1 A_2 \theta_d p_1^{1/2}} \left[ \frac{p_m^{1/2}(\theta_d + \theta_s, l)}{p_m^{1/2}(l)} + \frac{p_m^{1/2}(-\theta_d + \theta_s, l)}{p_m^{1/2}(l)} - \frac{2p_m^{1/2}(\theta_s, l)}{p_m^{1/2}(l)} \right] \quad (11)$$

where  $p_m(l)$  refers to the maximum pressure of the profile,

$$K = \frac{2A_2(l - \frac{w_2}{2})(1+\alpha_2)(1+\sin \varphi) \cos^2 \theta_s}{A_1 L(1+\alpha_1)\alpha_2}$$

and

$$Q_1 \equiv A_1 \sqrt{\frac{2g_c p_1}{\rho}}$$

and where it must be kept in mind that  $\frac{\partial p(\theta+\theta_s)}{\partial \theta_s} = \frac{\partial p(\theta+\theta_s)}{\partial \theta}$

#### 4.2 Pressure Gain

The pressure gain of a proportional fluid amplifier is defined as the ratio of change in total output pressure difference, to the change in total input pressure difference. This may be written as

$$G_p \equiv \frac{\Delta p_o}{\Delta p_i} \quad (12)$$

or

$$G_p \equiv \frac{\Delta(p_L - p_R)}{\Delta(p_2 - p_3)} \quad (12a)$$

The output pressure difference  $p_o$  is a function of the pressure profile,  $p(\theta, \theta_s)$ , the width of the apertures  $\theta_d$ , and the downstream distance of the apertures,  $\ell$ ; that is

$$p_o = p_o(\theta, \theta_s, \theta_d, \ell) \quad (13)$$

The total differential of equation (13) is

$$dp_o = \frac{\partial p_o}{\partial \theta} d\theta + \frac{\partial p_o}{\partial \theta_s} d\theta_s + \frac{\partial p_o}{\partial \theta_d} d\theta_d + \frac{\partial p_o}{\partial \ell} d\ell \quad (14)$$

For small increments, the pressure gain may now be written as

$$G_p = \frac{dp_o}{dp_i} = \frac{\partial p_o}{\partial \theta} \frac{d\theta}{dp_i} + \frac{\partial p_o}{\partial \theta_s} \frac{d\theta_s}{dp_i} + \frac{\partial p_o}{\partial \theta_d} \frac{d\theta_d}{dp_i} + \frac{\partial p_o}{\partial \ell} \frac{d\ell}{dp_i} \quad (15)$$

Assuming that the pressure profile does not change for small control inputs, and since  $\theta_d$  and  $L$  are independent of  $p_i$ , the gain expression reduces to

$$G_p = \frac{\partial p_o}{\partial \theta_s} \frac{d\theta_s}{dp_i} \quad (16)$$

From the assumptions, the output pressure is in the form of dynamic pressure; therefore,

$$p_o = \frac{\rho}{2g_c} v_{avL}^2 - \frac{\rho}{2g_c} v_{avR}^2 \quad (17)$$

By using the expression for average velocity, the output pressure difference is

$$p_o = \left[ \frac{1}{\theta_d} \int_0^{\theta_d} p^{1/2}(\theta + \theta_s, l) d\theta \right]^2 - \left[ \frac{1}{\theta_d} \int_{-\theta_d}^0 p^{1/2}(\theta + \theta_s, l) d\theta \right]^2 \quad (18)$$

The relation between stream deflection and input pressure difference is derived in appendix A. If the left and right control areas are equal, the relation is approximately

$$\tan \gamma = \frac{A_2(1+\alpha_2)(1+\sin \varphi) p_1}{A_1(1+\alpha_1)p_1} \quad (19)$$

From the geometrical relation in equation (10), equation (19) may be written as

$$\tan \theta_s = \frac{A_2(l - \frac{w_2}{2})(1+\alpha_2)(1+\sin \varphi) p_1}{A_1 L(1+\alpha_1)p_1} \quad (20)$$

A theoretical expression for pressure gain is obtained by combining equations (16), (18), (20), and normalizing the pressure so that

$$G_p = \frac{\alpha_2 K p_m(l)}{\theta_d p_1} \left\{ \left[ \frac{p^{1/2}(\theta_d + \theta_s, l)}{p_m^{1/2}(l)} - \frac{p^{1/2}(\theta_s, l)}{p_m^{1/2}(l)} \right] \left[ \frac{1}{\theta_d} \int_0^{\theta_d} \frac{p^{1/2}(\theta + \theta_s, l)}{p_m^{1/2}(l)} d\theta \right] - \left[ \frac{p^{1/2}(\theta_s, l)}{p_m^{1/2}(l)} - \frac{p^{1/2}(-\theta_d + \theta_s, l)}{p_m^{1/2}(l)} \right] \left[ \frac{1}{\theta_d} \int_{-\theta_d}^0 \frac{p^{1/2}(\theta + \theta_s, l)}{p_m^{1/2}(l)} d\theta \right] \right\} \quad (21)$$

where, as before,

$$K = \frac{2A_2(l - \frac{w_2}{2})(1+\alpha_2)(1+\sin \varphi) \cos^2 \theta_s}{A_1 L(1+\alpha_1)\alpha_2}$$

#### 4.3 Power Gain

The power gain may be defined in terms of pressure gain and flow gain, so that

$$G_{pQ} \equiv \left| \frac{\Delta p_o \Delta Q_o}{\Delta p_1 \Delta Q_1} \right| \quad (22)$$

or,

$$G_{pQ} = \left| G_p G_Q \right| \quad (22a)$$

The theoretical expression for power gain is, therefore, obtained by multiplying equation (11) by equation (21).

## 5. APPLICATION OF THEORY

### 5.1 Predicting the Gain of a Fluid Amplifier

The theoretical expressions for flow and pressure gain are given in equations (11) and (21). Gains are calculated from these equations by specifying:

- (a) The shape of the pressure profile at the entrance to the apertures;
- (b) The physical dimensions of the amplifier;
- (c) The ratio of dynamic pressure to total pressure for control ( $\alpha_2$ ) and power ( $\alpha_1$ ) streams; and
- (d) The turning angle of the control stream  $\phi$ .

Experimental (fig. 4) and theoretical analyses (ref 2) of 2-D submerged jets show that the pressure profile is approximately Gaussian in the region of established flow. This may be expressed mathematically as

$$p(\theta) \approx p_m \exp \left[ - \frac{(\theta - \theta_s)^2}{2\sigma^2} \right] \quad (23)$$

At power-stream pressures of 5 psig, and an aspect ratio of 8:1, these data gave a peak pressure  $p_m$  of 3.5 psig and a standard deviation  $\sigma$  of approximately 2.40 deg at 11 nozzle widths downstream. Since the value of  $\sigma$  depends to some extent on aspect ratio, the dependence of pressure and flow gains on  $\sigma$  is also considered.

The ratios  $\alpha_1$  and  $\alpha_2$  were determined experimentally as  $\alpha_1 = 0.84$  and  $\alpha_2 = 0.44$  at the operating pressures of the amplifier. These operating pressures were chosen below 5 psig so that the assumption of incompressibility would be valid.

The turning angle  $\phi$  has been taken as 8 deg, since the power stream spreads at approximately this angle in the interaction region. The direction of flow of the control stream as it leaves the interaction region therefore differs from the axis of the power stream by this angle.

When these  $\sigma$  values are employed in equations (11), (21), and (22), the theoretical flow, pressure, and power gains are determined. Figures 6, 7, and 8 show the theoretical gains plotted against deflection angle for a Gaussian profile.

## 5.2 Optimization of Gain

Consideration will now be given to the effect of varying certain physical dimensions of the amplifier to optimize the gain using measured pressure profiles.

It should be noted that the pressure gain given by equation (21) is not directly proportional to the ratio of control area  $A_2$  and power area  $A_1$  alone, since the  $Q$ 's are also functions of the areas. This applies also to the ratio of flow rates  $Q_2/Q_1$  in the flow gain expression (eq 11). Since the functional relation between the areas (or flow rates) and the  $Q$ 's is not analyzed here, the effects of varying the area ratio or flow rate control to power ratio is not considered.

### 5.2.1 Constant-Width Apertures—Varying Distance Downstream

As the downstream distance of constant-width apertures is increased, each aperture accepts a smaller percentage of the total stream. The peak pressure is also decreasing with increasing downstream distance. Using experimental profile data taken at DOFL, these quantities may be related to downstream distance. Figure 9 is a plot of theoretical pressure, flow, and power gains versus downstream distance for the case of a constant width aperture equal to 1.5 power nozzle widths and a stream deflection  $\theta_s = 0$ . The theoretical gains maximize at 11 nozzle widths downstream.

### 5.2.2 Constant-Deviation Apertures—Varying Distance Downstream

If the apertures are constrained to subtend a fixed angle, the aperture width must increase with increasing downstream distance. Figure 10 shows the relation between theoretical pressure, flow, and power gains, and downstream distance for a fixed aperture angle of 2.4 deg at a stream deflection of  $\theta_s = 0$ . The pressure gain decreases monotonically in the region of established flow, whereas the flow gain increases monotonically. The power gain, however, exhibits a maximum at about 11 nozzle widths downstream.

### 5.2.3 Varying-Width Apertures—Fixed Downstream Distance

Varying the width of apertures at a fixed downstream position varies their position with respect to the pressure profile. Figure 11 is a plot of theoretical pressure, flow, and power gains versus the equivalent  $\sigma$  width at 11 nozzle widths downstream and  $\theta_s = 0$ .

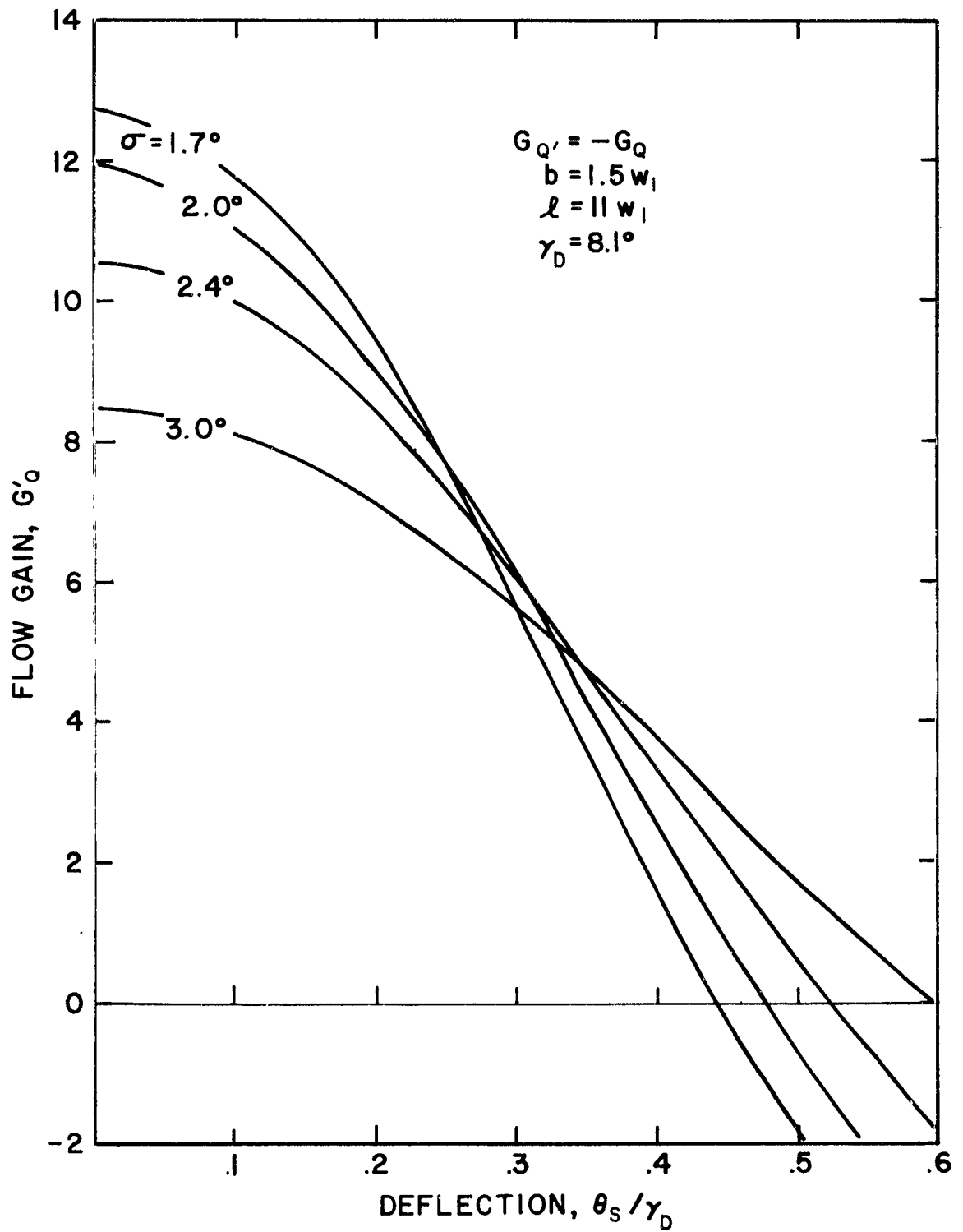


Figure 6. Theoretical flow gain versus stream deflection with stream width as a parameter.

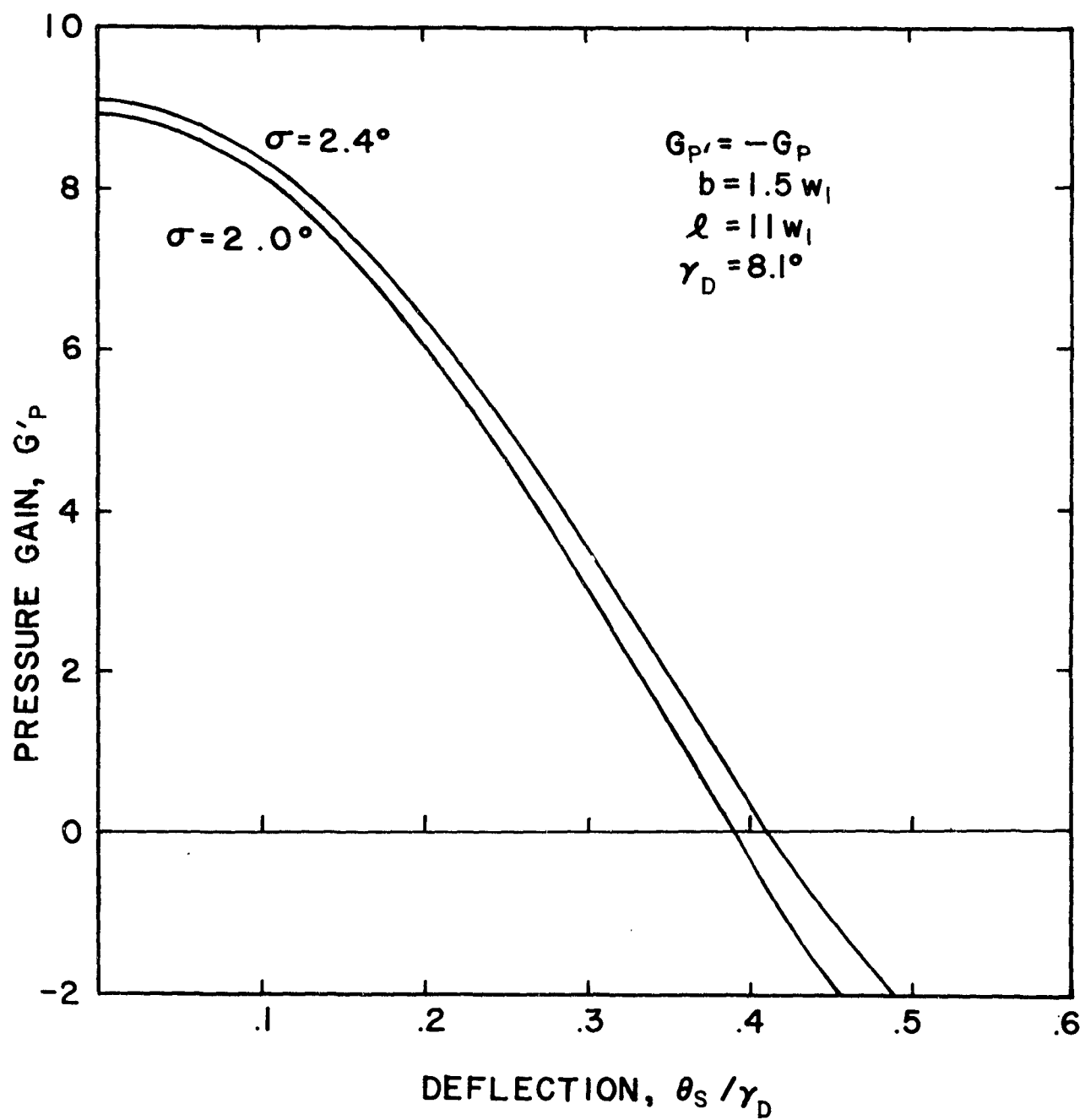


Figure 7. Theoretical pressure gain versus stream deflection with stream width as a parameter.

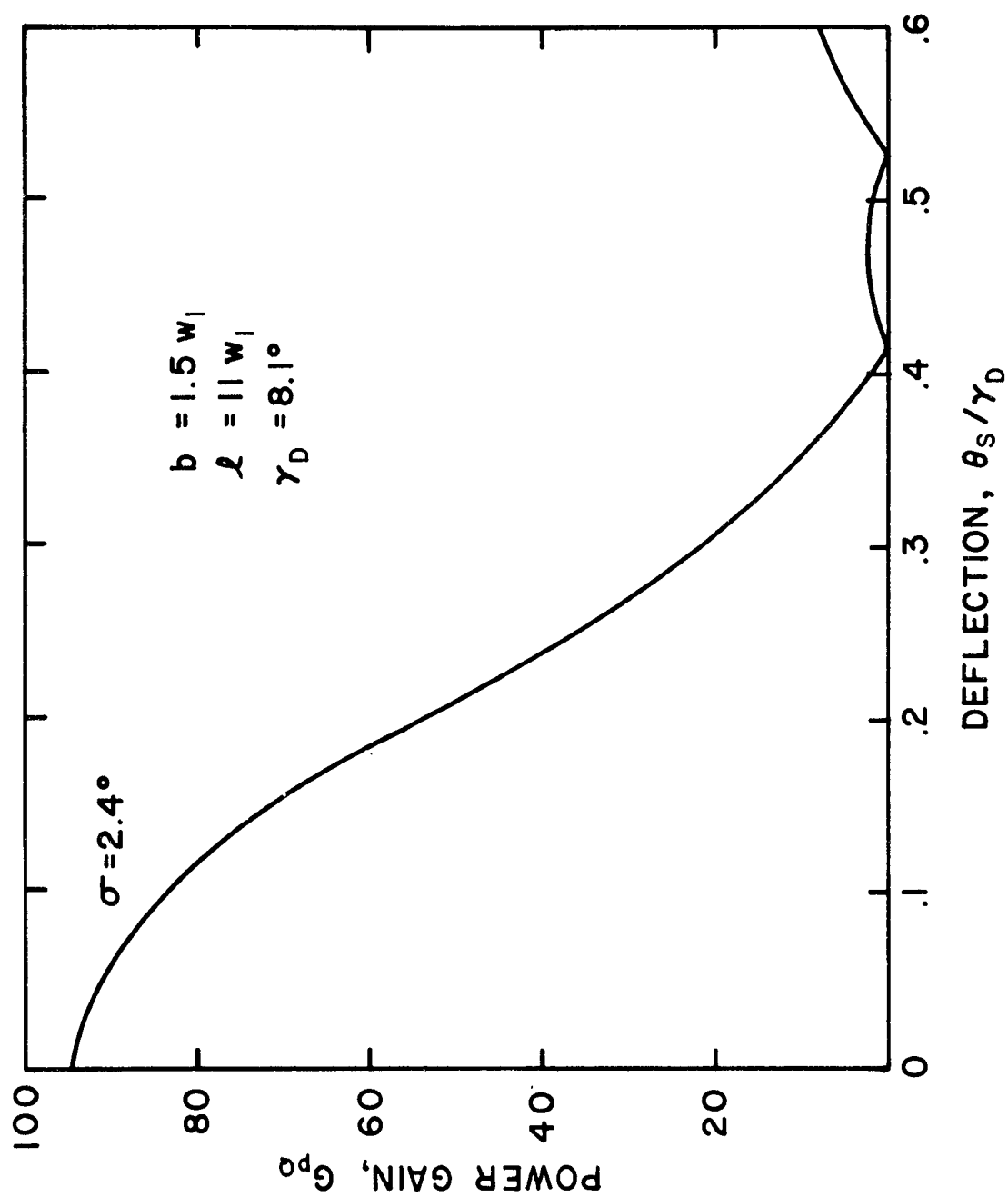


Figure 8. Theoretical power gain versus stream deflection with stream width as a parameter.

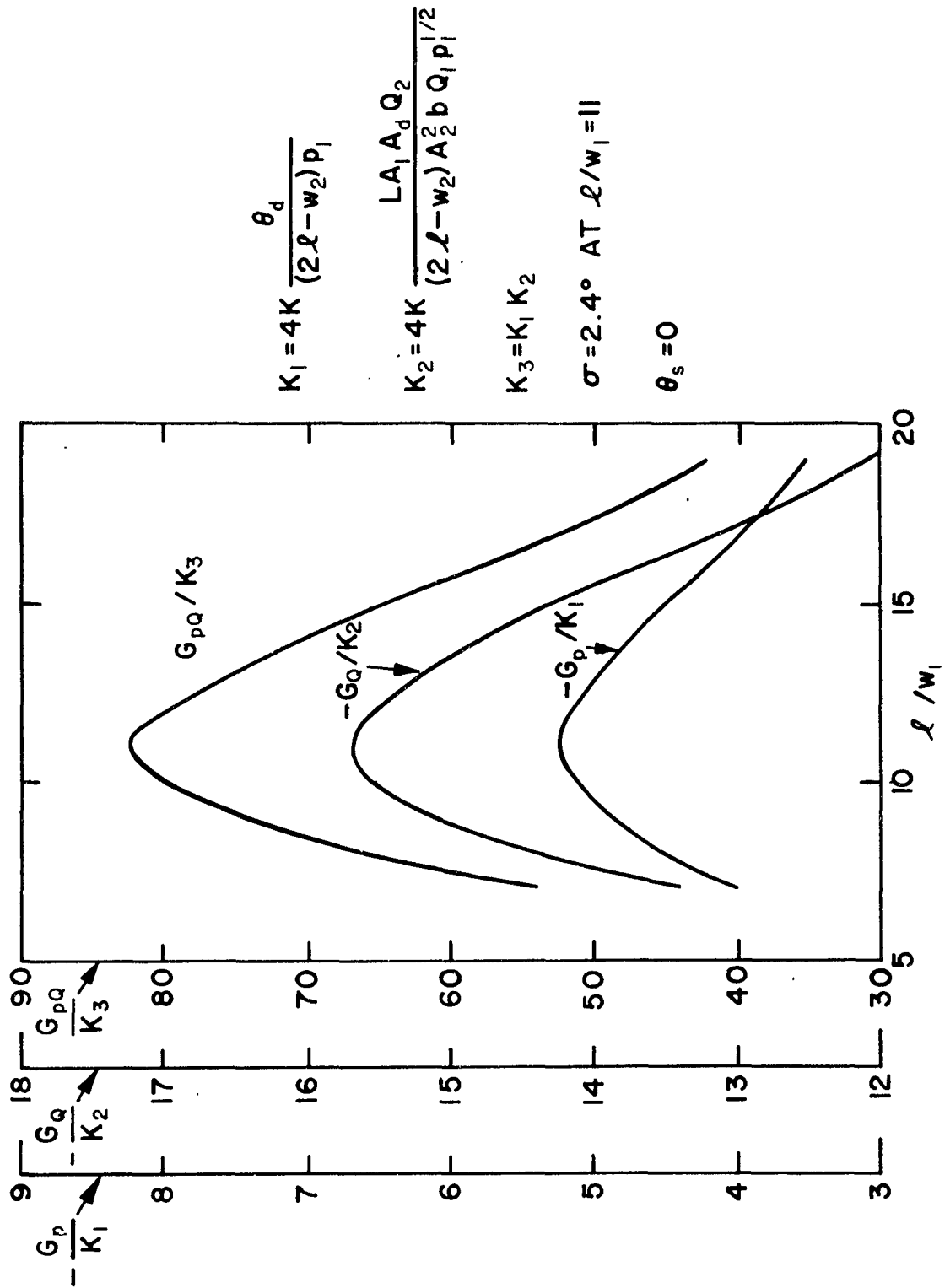


Figure 9. Theoretical gain versus downstream distance constant width aperture ( $\theta_s = 0$ ).

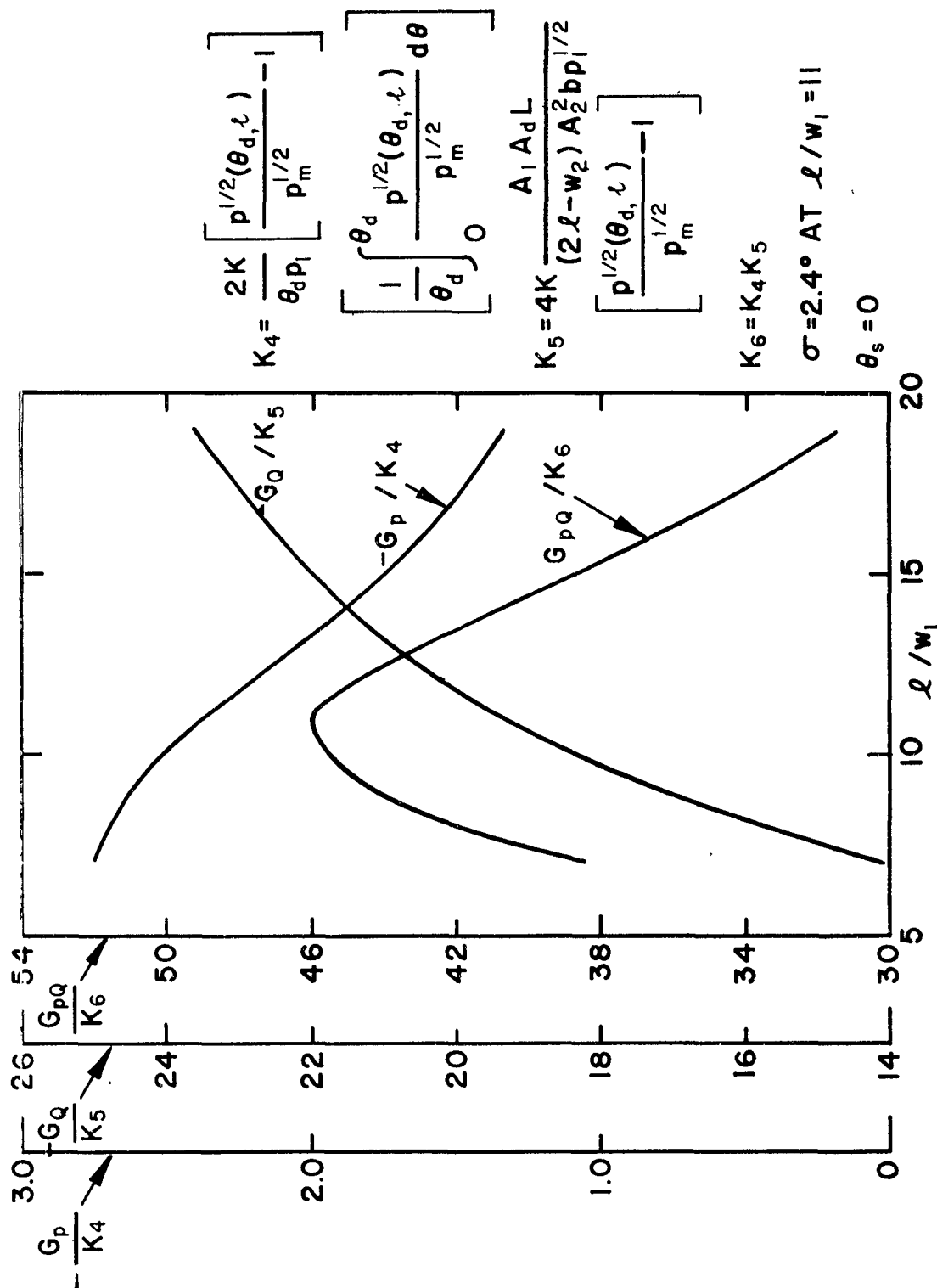


Figure 10. Theoretical gain versus downstream distance constant-deviation apertures ( $\theta_s = 0$ ).

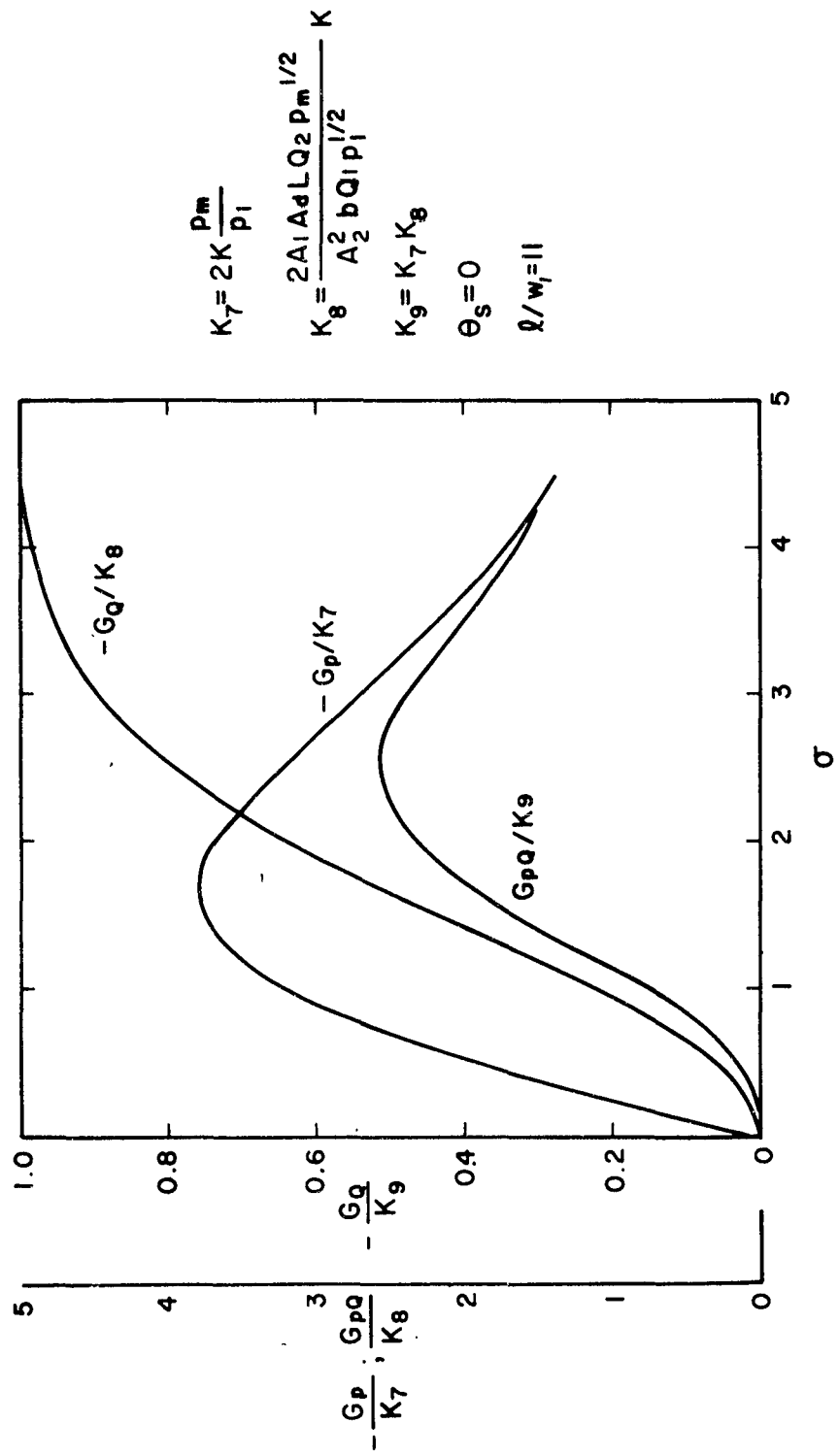


Figure 11. Theoretical gain versus aperture width fixed distance downstream ( $\theta_s = 0$ ).

The flow gain increases monotonically until the apertures increase to the width of the power stream; thereafter, increasing the aperture width does not change the gain. The pressure gain is a maximum at an aperture width of  $1.7\sigma$ , and the power gain is a maximum at approximately  $2.5\sigma$ .

## 6. TEST SETUP AND PROCEDURE

To check the theoretical analysis, tests were performed on the amplifier shown in figure 12. This amplifier has the following dimensional features:

- (a) The nozzle widths of power and control streams are approximately equal.
- (b) The entrance width  $b$  of each output aperture is 1.5 power nozzle widths.
- (c) The entrance of the apertures is fixed at 11 power nozzle widths from the exit of the power nozzle.
- (d) The ratio of nozzle height to power nozzle width (aspect ratio) is 8.

A functional diagram (fig. 13) shows the test arrangement used with this amplifier. The test setup consists of a regulated air supply to each nozzle and the means of measuring input and output conditions. The flow rate into the nozzles and out of the apertures is measured with rotameters that have a full-scale accuracy within 2 percent. The pressure in the control-input tanks is measured with manometers.

During a test, the power stream settling tank was maintained at a constant pressure of 3 or 5 psig. One of the control tanks was also kept at a constant pressure, which is 0 to 20 percent of the power-stream pressure. Small changes were then made in the other control pressure. The flowmeters at the input and output were read at each control-pressure point.

It may be seen in figure 12 that there are through-holes on each side of the power stream in the region between the control jets and apertures. This effectively short circuits any pressure difference across the stream, thereby insuring stream stability.

## 7. COMPARISON OF THEORETICAL AND EXPERIMENTAL RESULTS

In comparing the theoretical and experimental results, it is advantageous to plot output difference versus input difference rather than gain versus deflection angle, since calculation of experimental gain requires division by small differences, which reduces the accuracy of the results. Equations (2) and (12) show that the slope of the curve that has the output difference as ordinate and input difference as abscissa will be the gain of the amplifier.

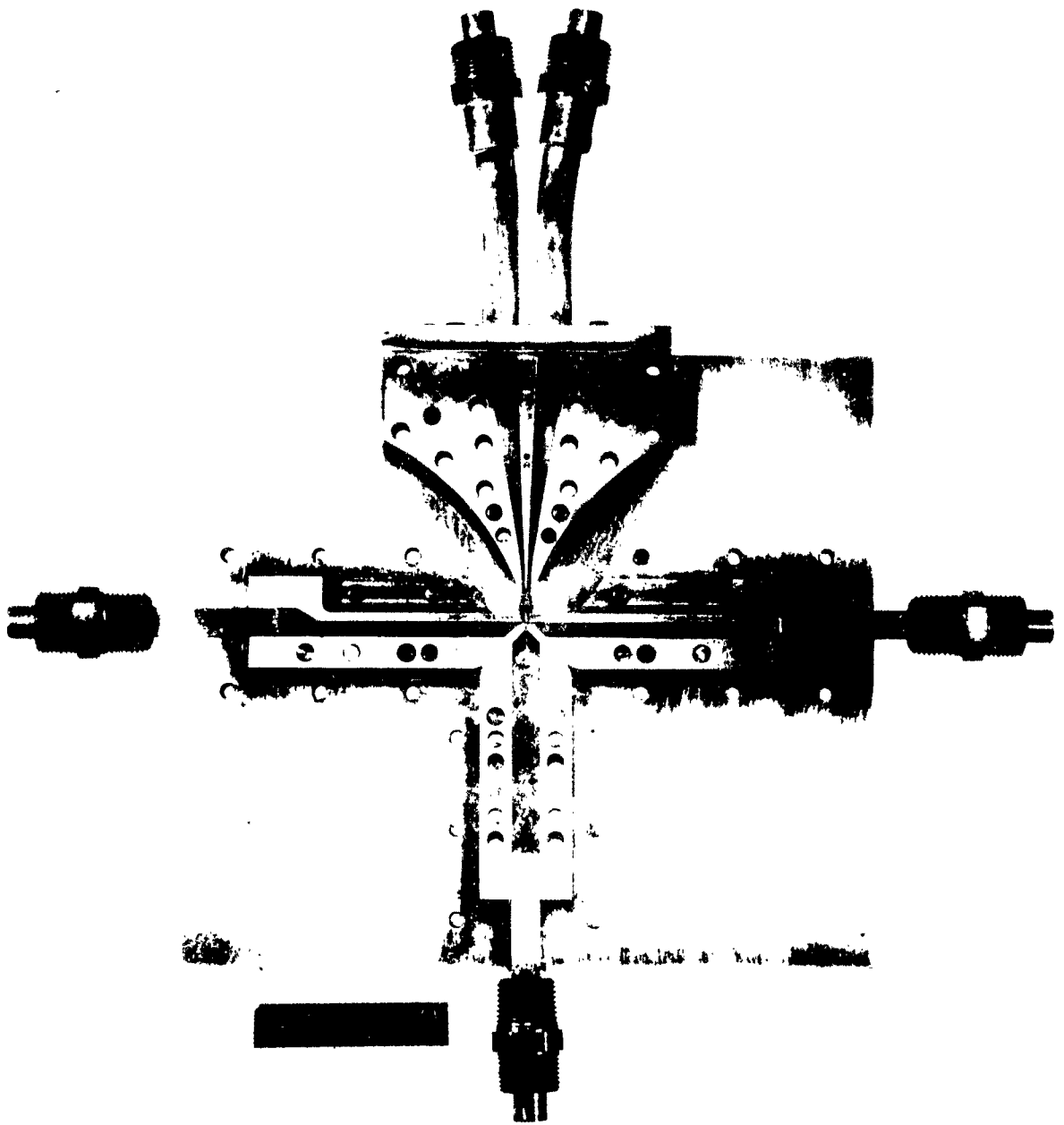


Figure 12. Proportional amplifier.

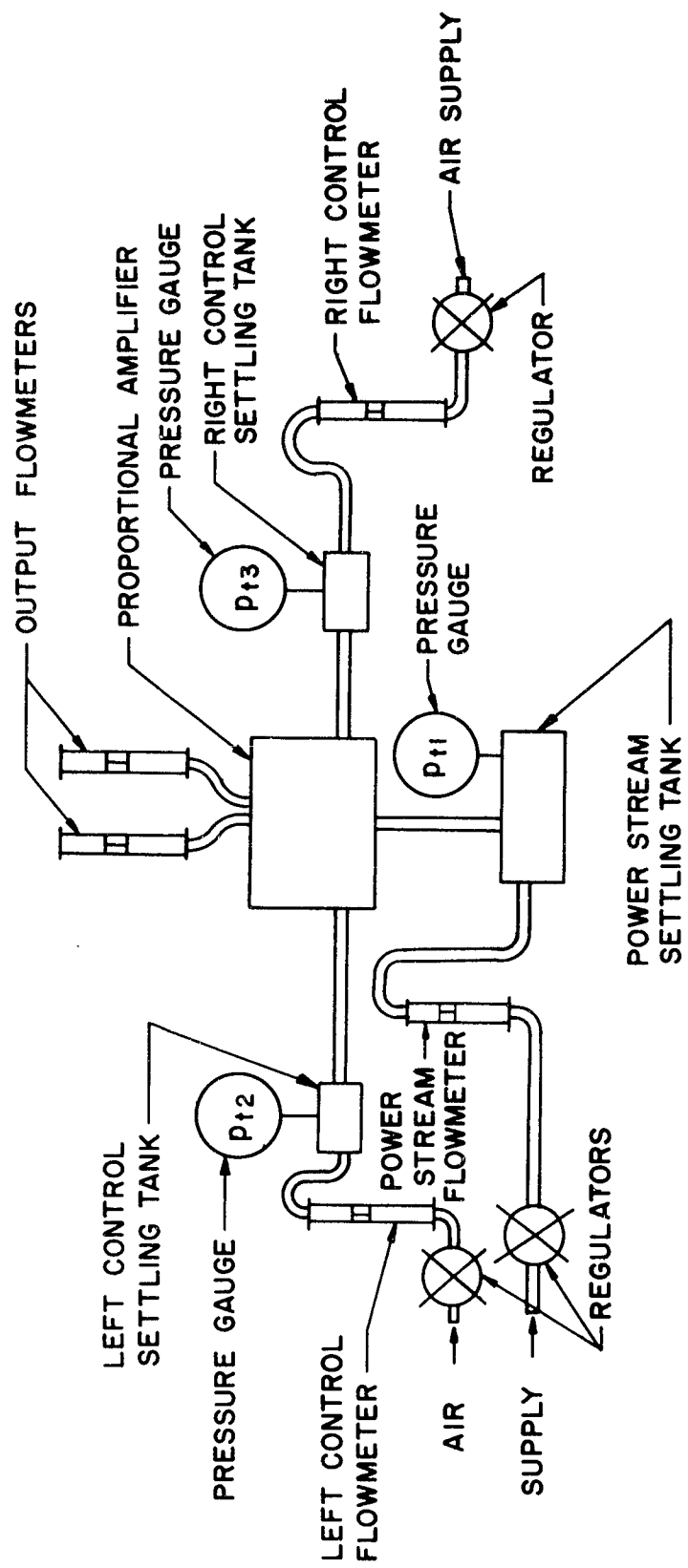


Figure 13. Functional diagram of test setup.

### 7.1 Flow Difference

If the conditions given in section 5.1 are assumed again, a theoretical relation between aperture-flow difference  $Q_L - Q_R$  and control-flow difference  $Q_2 - Q_3$  can be calculated from equations (8), (9), and (10). The theoretical and experimental flow difference results are shown in figures 14 and 15.

The theoretical and experimental results are in close agreement until the control flow difference reaches 10 percent of the power stream flow. As the control flow increases above this value, the experimental results become higher than predicted by the theory.

### 7.2 Pressure Difference

The theoretical relation between aperture pressure difference  $P_L - P_R$  and control pressure difference  $p_2 - p_3$  can be calculated from equations (18) and (20) by using the conditions given in section 5.1. This relation is shown in figures 16 and 17 for both theoretical and experimental results. In the experimental results, the dynamic pressure at the entrance to the apertures is computed from the output flowmeter readings by relating dynamic pressure to average velocity and using the equation of continuity.

The experimental and theoretical curves have essentially the same shape. For small control pressure differences, the agreement is good. As the control pressure difference increases, the experimental aperture pressure difference becomes larger than predicted by the theory. The maximum value, or point of zero gain, occurs when the control pressure difference is approximately 10 percent of the power stream pressure.

## 8. DISCUSSION

To obtain the theoretical output differences a Gaussian pressure profile was assumed. This profile was selected from those found experimentally by specifying the same standard deviation and maximum value. Increasing the standard deviation of the theoretical profile as much as 20 percent caused only a negligible change in the output difference functions,  $P_L - P_R$  and  $Q_L - Q_R$ , because all apertures were almost equally affected. This was also confirmed experimentally. The experimental profile was broadened by increasing the percentage of control pressure; however, tests made at 10-, 20-, and 30-percent control pressure yielded close results. If the maximum value of the Gaussian is changed, the output difference functions are also changed. According to the theory, the aperture difference pressure is directly proportional to the maximum pressure. The experiments made with power stream pressures of 3 psig and 5 psig tended to confirm this. At a

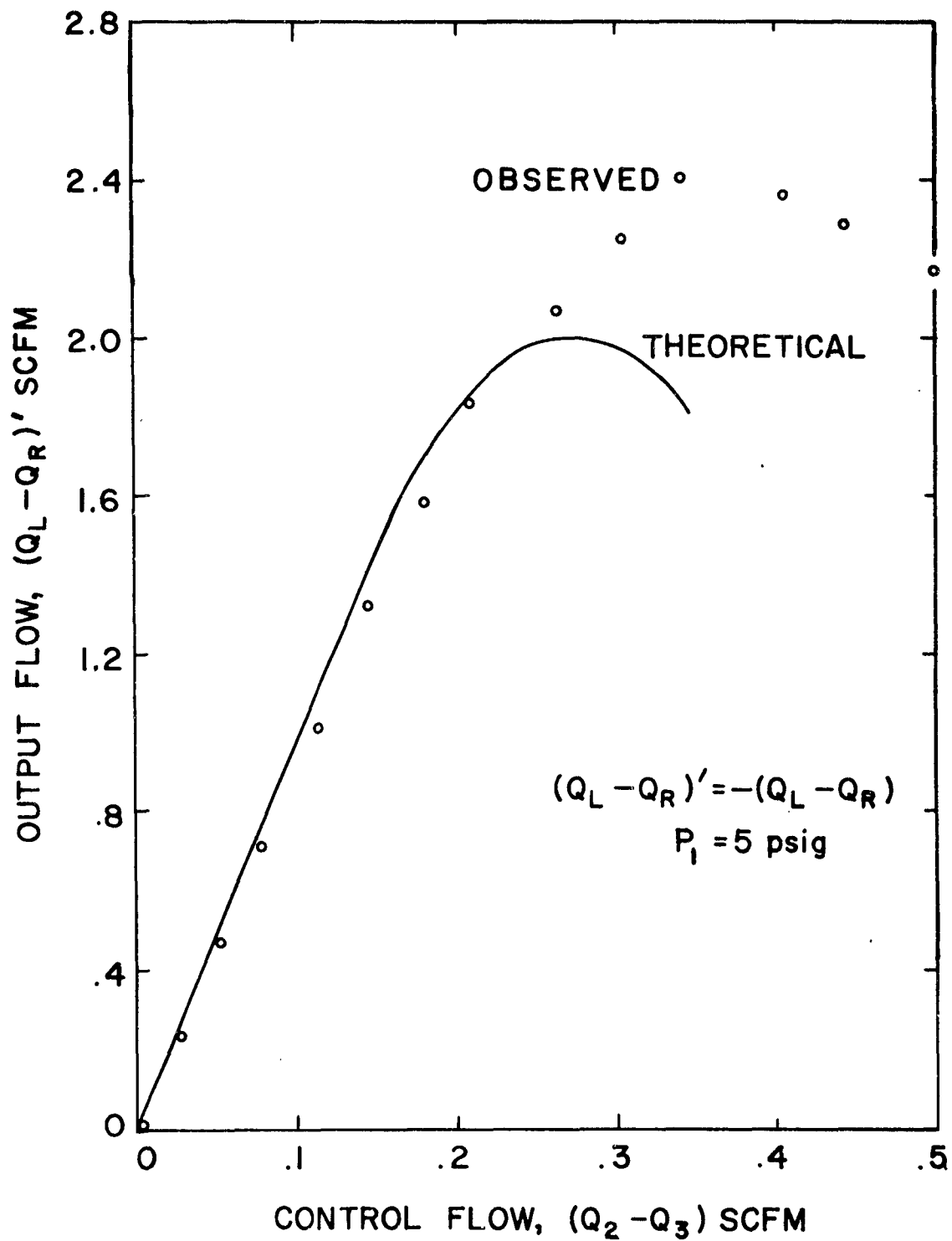


Figure 14. Comparison of experimental and theoretical flow differences.

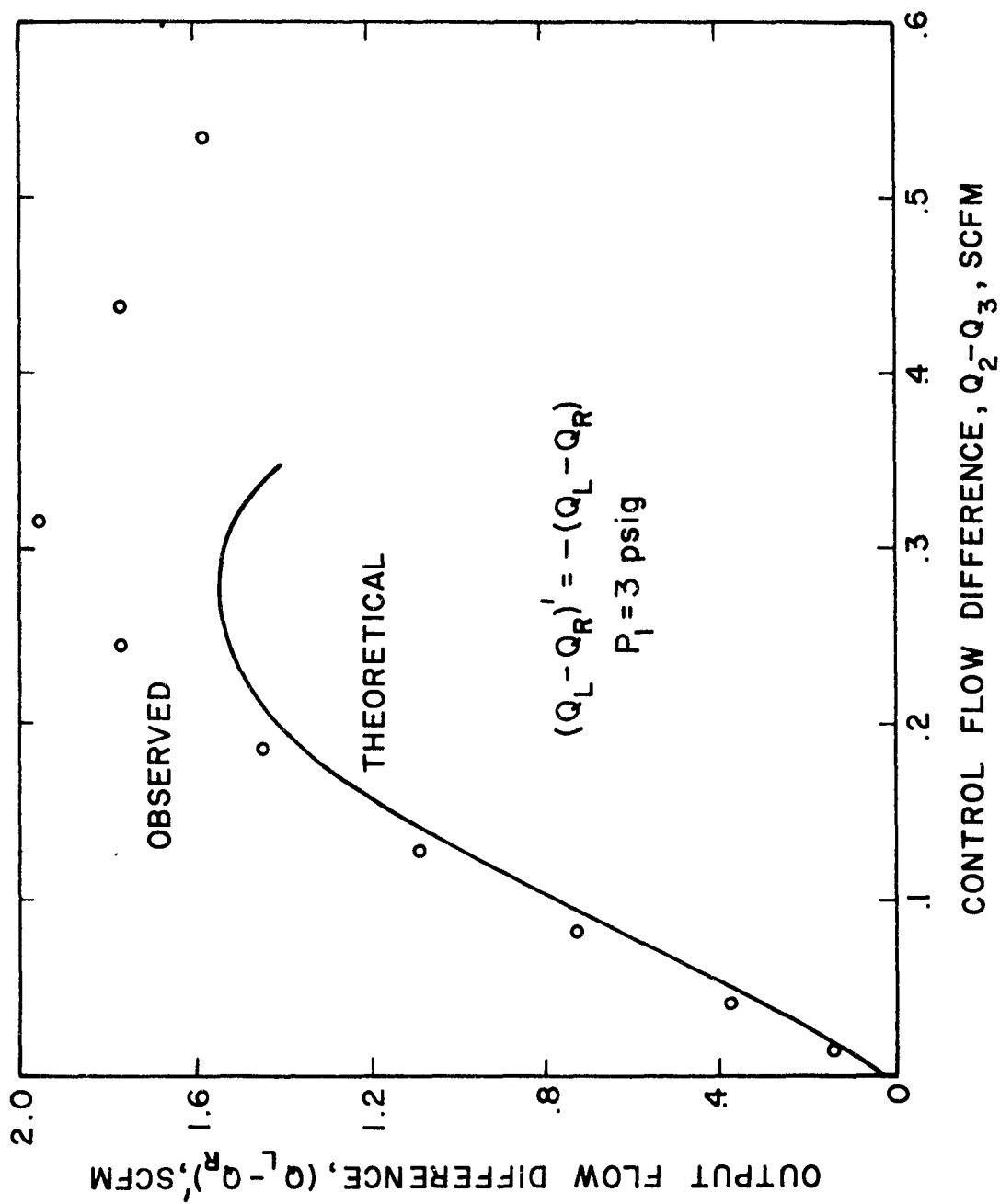


Figure 15. Comparison of experimental and theoretical flow differences.

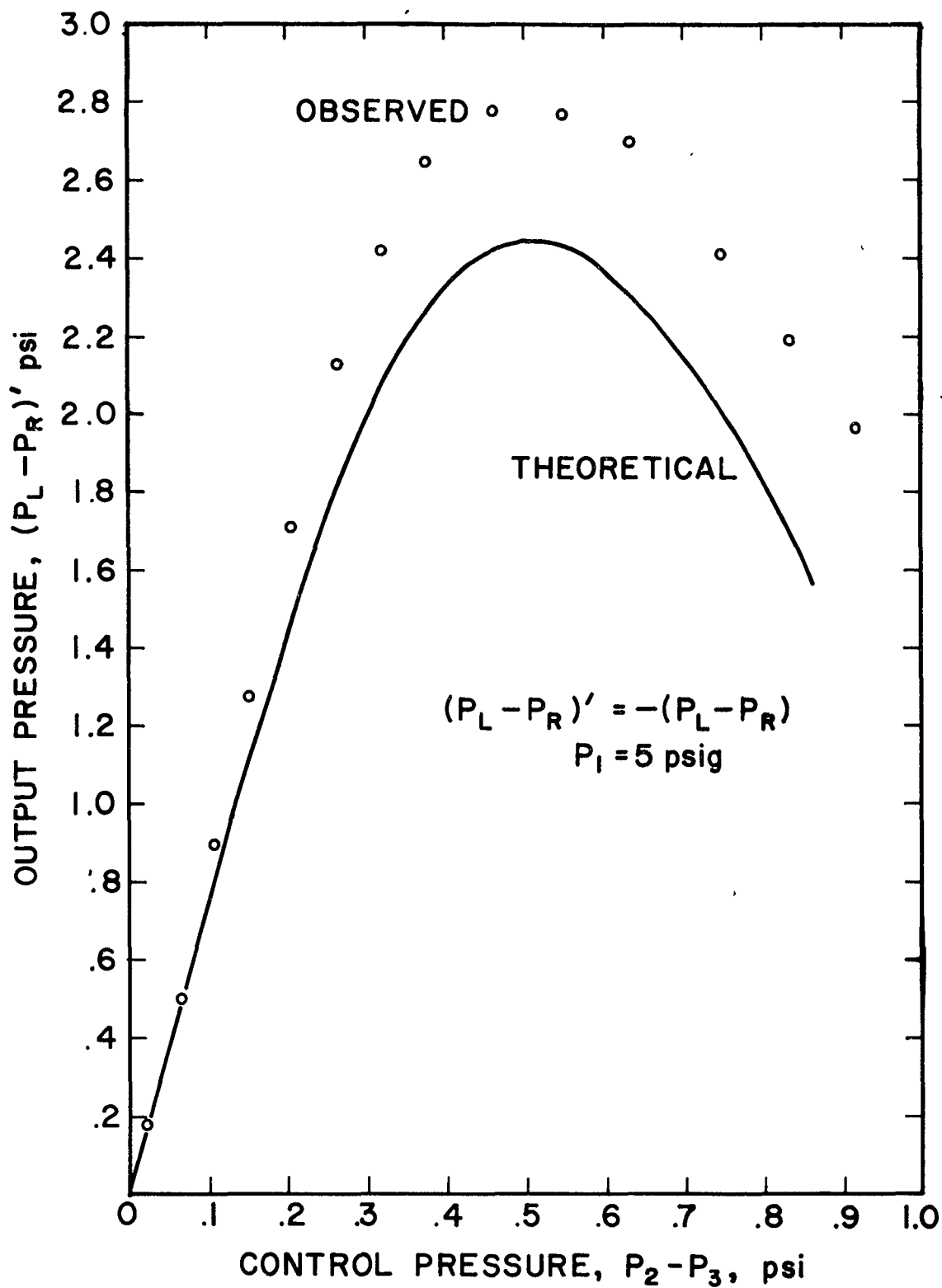


Figure 16. Comparison of experimental and theoretical pressure differences.

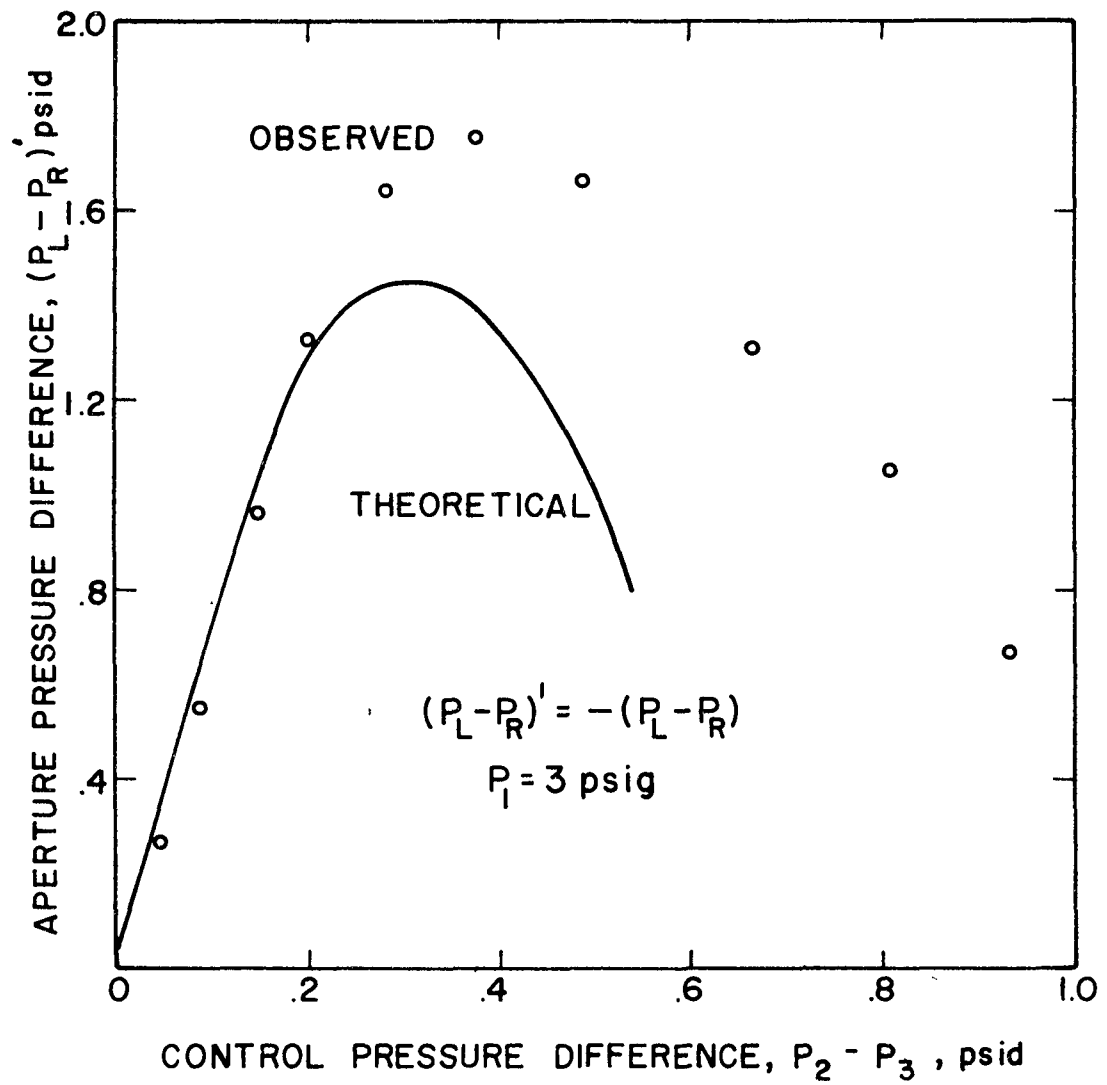


Figure 17. Comparison of experimental and theoretical pressure differences.

power stream pressure of 5 psig, the maximum aperture pressure difference was 2.78 psig. At 3 psig, the aperture pressure difference was 1.75 psig. The ratio of these is 0.63 compared with the prediction of 0.60 from the theory. In addition, experimental profile data of undeflected streams obtained at DOFL were substituted in the theoretical equations. The result was within 5 percent of the result obtained with the Gaussian profile. It must be concluded, then, that the use of Gaussian profiles in place of actual undeflected profiles leads to relatively small errors in the theoretical results.

To obtain the theoretical input differences, the momentum equation was applied to the interaction region (app A). An approximate relation has been employed to give the input-pressure difference  $p_2 - p_3$  in equation (20) and the input-flow difference  $Q_2 - Q_3$  from equation (9). At present there are no experimental data available to check the accuracy of this relation.

As the control differences increase, the experimental output differences become greater than the theory predicts. The theoretical output differences were based on the assumption of a Gaussian profile. At present, profiles of highly deflected streams have not been taken but they are not expected to remain Gaussian; therefore, the use of a profile that remains Gaussian restricts the theoretical results to conditions where the steam deflections are small.

The experimental difference functions are greater than the theory predicts. In the present tests the total output flow was greater than the profile indicated, even when the stream was not deflected. This occurs because a fluid whose velocity is nonuniform at the input to an aperture continues to entrain fluid after the fluid has entered the collectors. In this analysis, all calculations were made under the assumption that the velocity profile at the input to an aperture is unaffected by the presence of the aperture.

## 9. CONCLUSIONS

A theory has been presented that predicts small signal pressure, flow, and power gain of a single amplifier stage. The theory indicates that a power gain of about 100 is easily achievable with pressure and flow gains of about 10.

All gains are at maximum when the power stream is evenly divided by the two output apertures. The gains decrease with deflection angle and become zero when the stream is approximately centered in one of the apertures.

The power gain maximizes at about 11 power-jet nozzle widths downstream with aperture widths 1.5 times the power-jet nozzle width.

Comparison of those aspects of the theory, which could be checked on a single laboratory model showed good agreement within the experimental error. On this model the pressure gain was calculated to be 9.1 and measured 8.4; the flow gain was calculated to be 10.5 and measured 9.4.

#### 10. REFERENCES

(1) DOFL TR-1039, "Fluid Amplification—No. 1: Basic Principles," R. W. Warren and S. J. Peperone, 15 Aug 1962 (Part II).

(2) M. J. Albertson, Y. B. Dai, R. A. Jensen and H. Rouse, "Diffusion of Submerged Jets," Proc. Am. Soc. Civ. Engrs., Dec 1948.

(3) B. G. Newman, "The Deflection of Plane Jets by Adjacent Boundaries—Coanda Effect," Pergamon Press, 1961 (Boundary Layer and Flow Control, Vol 1).

(4) Prandtl and Tietjens, "Fundamentals of Hydro- and Aeromechanics," Dover Publications, Inc (1957).

## APPENDIX A

### THEORETICAL ANALYSIS OF INTERACTING STREAMS—MATHEMATICAL DERIVATIONS

To formulate the expression for gain in equation (6) and (16), it is necessary to have a relationship between input difference and the stream deflection. This relation can be obtained by the application of the momentum equation to the control and power streams.

In the derivation it is assumed that the fluid is incompressible, the flow is steady, there is no energy loss, and the change in momentum is due only to the change in direction of the interacting streams. Experiments have shown that the axes of the power stream and control streams are not parallel after interacting because of the characteristic spreading of a jet stream. This fact is considered in the derivation.

From the above assumptions and neglecting body forces, the momentum equation

$$-\int_{\text{Area}} p_s d\vec{A} = \int_{\text{Area}} \frac{\rho}{g_c} (\vec{v} \cdot d\vec{A}) \vec{v} \quad (\text{A-1})$$

may be written as Newton's second law

$$\sum \vec{F} = \frac{d\vec{M}}{dt} \equiv \dot{\vec{M}} \quad (\text{A-2})$$

where  $\vec{M}$  is the momentum vector and  $\vec{F}$  is the force vector.

From the free body diagrams shown in figure A-1, the following component equations are obtained (where the subscript w denotes the wall):

#### Left-Control Stream

$$\sum F_x = \dot{M}_x$$

$$p_{s2} A_2 \cos \beta + p_{s2} A_2 \sin(\varphi - \gamma) - F_{x2} = - \frac{\rho}{g_c} A_2 v_2^2 \sin(\varphi - \gamma) - \frac{\rho}{g_c} A_2 v_2^2 \cos \beta \quad (\text{A-3})$$

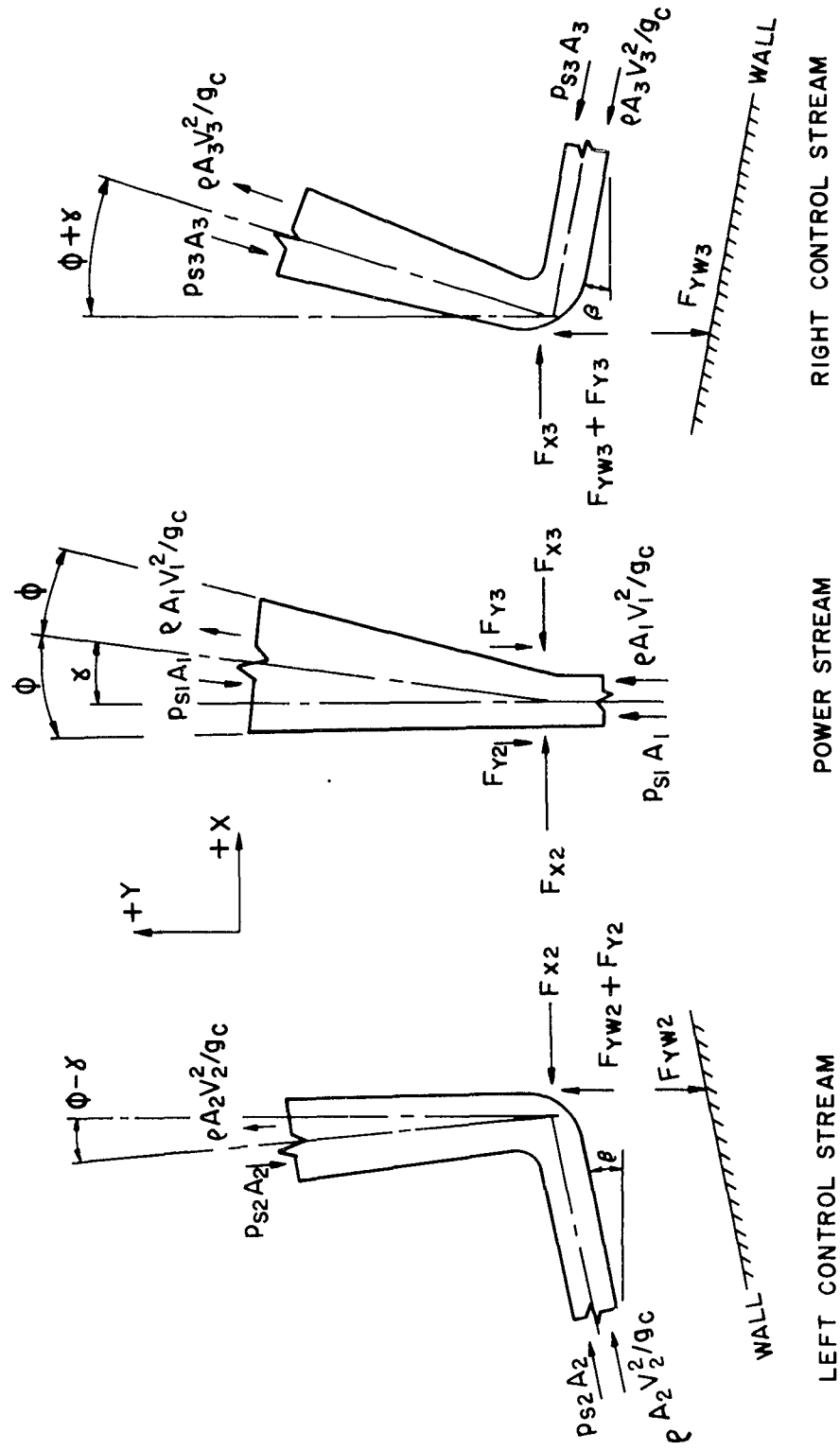


Figure A-1. Free body diagrams of the interacting streams.

$$\sum F_y = \dot{M}_x$$

$$p_{s2} A_2 \sin \beta + F_{yw2} + F_{y2} - p_{s2} A_2 \cos(\varphi - \gamma) = \frac{\rho}{g_c} A_2 v_2^2 \cos(\varphi - \gamma) - \frac{\rho}{g_c} A_2 v_2^2 \sin \beta \quad (A-4)$$

#### Right-Control Stream

$$\sum F_x = \dot{M}_x$$

$$F_{x3} - p_{s3} A_3 \cos \beta - p_{s3} A_3 \sin(\varphi + \gamma) = \frac{\rho}{g_c} A_3 v_3^2 \sin(\varphi + \gamma) + \frac{\rho}{g_c} A_3 v_3^2 \cos \beta \quad (A-5)$$

$$\sum F_y = \dot{M}_y$$

$$p_{s3} A_3 \sin \beta + F_{yw3} + F_{y3} - p_{s3} A_3 \cos(\varphi + \gamma) = \frac{\rho}{g_c} A_3 v_3^2 \cos(\varphi + \gamma) - \frac{\rho}{g_c} A_3 v_3^2 \sin \beta \quad (A-6)$$

#### Power Stream

$$\sum F_x = \dot{M}_x$$

$$F_{x2} - F_{x3} - p_{s1} A_1 \sin \gamma = \frac{\rho}{g_c} A_1 v_1^2 \sin \gamma \quad (A-7)$$

$$\sum F_y = \dot{M}_y$$

$$p_{s1} A_1 + \frac{\rho}{g_c} A_1 v_1^2 - F_{y2} - F_{y3} - p_{s1} A_1 \cos \gamma = \frac{\rho}{g_c} A_1 v_1^2 \cos \gamma \quad (A-8)$$

#### Wall

$$F_{yw3} = p_{s3} A_3 \quad ; \quad F_{yw2} = p_{s2} A_2 \quad (A-9)$$

Now, if eq (A-7) is divided by eq (A-8)

$$\tan \gamma = \frac{F_{x2} - F_{x3}}{p_{s1} A_1 + \frac{\rho}{g_c} A_1 v_1^2 - F_{y2} - F_{y3}} \quad (A-10)$$

Substituting equations (A-3), (A-4), (A-5), (A-6), and (A-9) into (A-10) the result is

$$\tan \gamma = \frac{[p_{s2}A_2 + \frac{\rho}{g_c} A_2 v_2^2][\cos \beta + \sin(\varphi - \gamma)] - [p_{s3}A_3 + \frac{\rho}{g_c} A_3 v_3^2][\cos \beta + \sin(\varphi + \gamma)]}{[p_{s1}A_1 + \frac{\rho}{g_c} A_1 v_1^2] + [p_{s2}A_2 + \frac{\rho}{g_c} A_2 v_2^2][\sin \beta - \cos(\varphi - \gamma)] + [p_{s3}A_3 + \frac{\rho}{g_c} A_3 v_3^2][\sin \beta - \cos(\varphi + \gamma)] + p_{s2}A_2 + p_{s3}A_3} \quad (A-11)$$

In general, the control streams are perpendicular to the power stream ( $\beta = 0$ ) so that equation (A-11) becomes

$$\tan \gamma = \frac{A_2[p_{s2} + \frac{\rho}{g_c} v_2^2][1 + \sin(\varphi - \gamma)] - A_3[p_{s3} + \frac{\rho}{g_c} v_3^2][1 + \sin(\varphi + \gamma)]}{A_1[p_{s1} + \frac{\rho}{g_c} v_1^2] - A_2[p_{s2} + \frac{\rho}{g_c} v_2^2][\cos(\varphi - \gamma)] - A_3[p_{s3} + \frac{\rho}{g_c} v_3^2][\cos(\varphi + \gamma)] + p_{s2}A_2 + p_{s3}A_3} \quad (A-12)$$

For power-stream deflection angles  $\gamma$  small compared with  $\varphi$ , the stream deflection is approximately

$$\tan \gamma = \frac{[A_2(p_{s2} + \frac{\rho}{g_c} v_2^2) - A_3(p_{s3} + \frac{\rho}{g_c} v_3^2)][1 + \sin \varphi]}{A_1[p_{s1} + \frac{\rho}{g_c} v_1^2] + \{p_{s2}A_2 + p_{s3}A_3 - [A_2(p_{s2} + \frac{\rho}{g_c} v_2^2) + A_3(p_{s3} + \frac{\rho}{g_c} v_3^2)] \cos \varphi\}} \quad (A-13)$$

In the denominator of equation (A-13), the bracketed term is at least an order of magnitude smaller than the first term. Neglecting this term leads to the further approximation

$$\tan \gamma = \frac{[A_2(p_{s2} + \frac{\rho}{g_c} v_2^2) - A_3(p_{s3} + \frac{\rho}{g_c} v_3^2)][1 + \sin \varphi]}{p_{s1}A_1 + \frac{\rho}{g_c} A_1 v_1^2} \quad (A-14)$$

Using Bernoulli's equation

$$p = p_s + \frac{\rho}{2g_c} v^2 \quad (A-15)$$

equation (A-14) becomes

$$\tan \gamma = \frac{[A_2(p_2 + \frac{\rho}{2g_c}v_2^2) - A_3(p_3 + \frac{\rho}{2g_c}v_3^2)][1 + \sin \phi]}{A_1(p_1 + \frac{\rho}{2g_c}v_1^2)} \quad (A-16)$$

If  $A_2 = A_3$  equation (A-16) takes the form in equation (19) with  $p_1 = p_2 - p_3$ ; that is,

$$\tan \gamma = \frac{A_2(1+\alpha_2)(1+\sin \phi)(p_1)}{A_1(1+\alpha_1)p_1} \quad (A-17)$$

where, by definition

$$\alpha_1 \equiv \frac{\rho v_1^2}{2g_c p_1} \quad ; \quad \alpha_2 = \alpha_3 \equiv \frac{\rho v_2^2}{2g_c p_2} \equiv \frac{\rho v_3^2}{2g_c p_3}$$

For the flow-gain expression, it is convenient to express equation (A-17) in terms of control flow rather than control pressure.

Expressing  $p_2$  and  $p_3$  in terms of  $\alpha_2$ ,  $v_2$  and  $v_3$  and still assuming that  $A_2 = A_3$ , gives

$$p_2 - p_3 = \frac{\rho}{2g_c \alpha_2} (v_2^2 - v_3^2) = \frac{\rho}{2g_c \alpha_2 A_2^2} (Q_2^2 - Q_3^2) \quad (A-18)$$

By definition  $Q_1 = Q_2 - Q_3$  so that

$$p_2 - p_3 = \frac{\rho}{2g_c \alpha_2 A_2^2} (Q_1^2 + 2Q_1 Q_3) \quad (A-19)$$

Substituting equation (A-19) for  $p_1$  in equation (A-17) gives

$$\tan \gamma = \frac{\rho(1+\alpha_2)(1+\sin \phi)(Q_1^2 + 2Q_1 Q_3)}{2g_c \alpha_2 A_1 A_2 (1+\alpha_1)p_1} \quad (A-20)$$

which is equivalent to equation (9).

## **DISTRIBUTION**

**Office of the Director of Defense Research & Engineering**  
**AMC Detachment No. 1, Temporary Bldg I**  
**Attn: Technical Library (2 copies)**

**Commandant**  
**U.S. Army Artillery & Guided Missile School**  
**Fort Sill, Okla**  
**Attn: Combat Development Department**

**Commander**  
**U.S. Naval Ordnance Laboratory**  
**White Oak, Silver Spring 19, Md.**  
**Attn: Technical Library (2 copies)**

**Commanding General**  
**White Sands Missile Range**  
**White Sands, New Mexico**  
**Attn: ORDES-OM, Tech Library**

**Commanding Officer**  
**Watervliet Arsenal**  
**Watervliet, New York**  
**Attn: Technical Library**

**Transportation Research Command**  
**Ordnance Liaison Officer**  
**Fort Eustis, Va.**

**Commanding Officer**  
**Picatinny Arsenal**  
**Dover, New Jersey**  
**Attn: Technical Library (3 copies)**

**Commanding General**  
**Ordnance Weapons Command**  
**Rock Island, Ill**  
**Attn: Technical Library**

**Ordnance Technical Intelligence Agency**  
**Arlington Hall Station**  
**Arlington 12, Virginia**  
**Attn: Technical Library**

**Commanding Officer**  
**Ordnance Special Weapons**  
**Ammunition Command**  
**Dover, New Jersey**  
**Attn: Technical Library**

DISTRIBUTION (Cont'd)

Commanding Officer  
Army Research Office (DURHAM)  
Box CM, Duke Station  
Durham, N. C.

Commanding General  
U.S. Army Ordnance Missile Command  
Redstone Arsenal, Alabama  
Attn: Technical Library (3 copies)  
Attn: ORDXM-REE, Bldg 7446, Charles Schriener

Commanding General  
Aberdeen Proving Ground  
Branch 3, Bldg 400  
Aberdeen, Maryland  
Attn: Tech Library (4 copies)

U.S. Army Artillery Board  
Missile Division  
Fort Bliss, Texas  
Attn: Technical Library

U.S. Naval Underwater Sound Laboratory  
Fort Trumbull  
New London, Conn.  
Attn: Technical Library  
Attn: Research Division, Dr. R. Berman

Department of the Navy  
Chief, Office of Naval Research  
Washington 25, D. C.

Department of the Navy  
RRRE-3L  
Bureau of Naval Weapons  
Washington 25, D. C.  
Attn: S. J. German

Commander  
Naval Ordnance Laboratory  
White Oak, Silver Spring, Maryland  
Attn: B. Gilbert

Commander  
U.S. Naval Ordnance Laboratory  
Corona, California  
Attn: Technical Library

Commander  
U.S. Naval Ordnance Test Station  
China Lake, California  
Attn: Technical Library

**DISTRIBUTION (Cont'd)**

Commanding Officer  
Ordnance Materials Research Office  
Watertown Arsenal  
Watertown 72, Mass.  
Attn: Director's Office

Director, Special Weapons  
Office of the Chief of Research & Development  
Department of the Army  
Washington 25, D. C.

Commanding General  
U.S. Army Electronics Proving Ground  
Fort Huachuca, Arizona  
Attn: Technical Library

Director, Army Research Office  
Office of the Chief of Research & Development  
Department of the Army  
Washington 25, D. C.  
Attn: Technical Library

Commanding Officer  
Department of the Army  
Springfield Armory  
Springfield 1, Mass.  
Attn: TIU

Commanding Officer  
AMC Detachment No. 1 Temporary Bldg 1  
Washington 25, D. C.  
Attn: ORDTU  
Attn: ORDTS  
Attn: ORDTN  
Attn: ORDTB  
Attn: ORDTX  
Attn: ORDTW

Commanding General  
Headquarters, U.S. CONARC  
Materials Developments Section  
Fort Monroe, Virginia  
Attn: MD-1

Commanding Officer  
New York Ordnance District  
770 Broadway  
New York 3, N. Y.  
Attn: William P. Blake

**DISTRIBUTION (Cont'd)**

Commanding Officer  
Los Angeles Ordnance District  
55 S. Grand Avenue  
Pasadena, California  
Attn: V. V. Barker

Commanding Officer  
Frankford Arsenal  
Philadelphia 37, Pennsylvania  
Attn: Reference Librarian (3 copies)

Commanding General  
Engineering Research & Development Laboratory  
Fort Belvoir, Virginia  
Attn: Technical Library

Department of the Army  
Office of the Chief of Research & Development  
Washington 25, D. C.  
Attn: Chief, Combat Material Div

Department of the Army  
Army Research Office  
The Pentagon, Washington 25, D. C.  
Attn: Lt Col J. T. Brown, Office, Chief of R & D

Commanding General  
OTAC  
Detroit Arsenal  
Centerline, Mich  
Attn: Technical Library

Commandant  
Command & General Staff College  
Archives  
Fort Leavenworth, Kansas

Commanding Officer  
Chemical Warfare Laboratories  
Army Chemical Center, Md.  
Attn: Technical Library

Commanding Officer  
Camp Detrick  
Frederick, Maryland

Commanding Officer  
U.S. Army Signal Research & Development Laboratory  
Fort Monmouth, N. J.  
Attn: Technical Library  
Attn: Arthur Daniel

**DISTRIBUTION (Cont'd)**

Commander  
Naval Research Laboratory  
Washington 25, D. C.  
Attn: Technical Library

Commandant  
U.S. Marine Corps  
Code A04F  
Washington 25, D. C.

Department of the Navy  
Bureau of Naval Weapons  
Washington 25, D. C.  
Attn: Code CACF-3

Department of the Navy  
Chief of Naval Operations  
R & D Planning Group  
The Pentagon, Washington 25, D. C.

Commander  
Aeronautical Systems Division  
Wright-Patterson Air Force Base, Ohio  
Attn: Technical Library

Department of the Air Force  
Deputy Chief of Staff for Development  
Director of R & D  
The Pentagon, Washington 25, D. C.

Commander  
Armed Services Technical Information Agency  
Arlington Hall Station  
Arlington 12, Virginia  
Attn: TIPDR (10 copies)

Commander  
Armed Services Technical Intelligence Agency  
Arlington Hall Station  
Arlington 12, Virginia  
Attn: TIPDR-B

Commander  
Air Research & Development Command  
Andrews Air Force Base  
Washington 25, D. C.  
Attn: Technical Library - B

DISTRIBUTION (Cont'd)

Commander  
Air Proving Ground Center  
Eglin Air Force Base, Florida  
Attn: Technical Library

Commander  
Air Material Command  
Wright-Patterson Air Force Base, Ohio  
Attn: LMDN

Air Force Systems Command  
Space Systems Division  
Los Angeles, 45, California  
Attn: Technical Data Center

Commander  
Air Force Ballistic Missile Division  
Inglewood, California  
P.O. Box 262  
Attn: WDSOT

Air Force Special Weapons Center  
Kirtland Air Force Base  
Albuquerque, New Mexico

Aeronautical Systems Division  
Wright-Patterson Air Force Base, Ohio  
Attn: WWRMOO (M. Schorr)

Scientific and Technical Information Facility  
P. O. Box 5700  
Bethesda, Maryland  
Attn: NASA Representative (S-AK/DL)  
National Aeronautics & Space Administration  
Langley Research Center  
Langley, Station, Hampton, Va.  
Attn: Technical Library

National Aeronautics & Space Agency  
Lewis Research Center  
2100 Brookpark Road  
Cleveland 35, Ohio  
Attn: K. Hiller

Marshall Space Flight Center  
Advanced Propulsion Section  
Huntsville Alabama  
Attn: M-S&M-PA

**DISTRIBUTION (Cont'd)**

**Marshall Space Flight Center**  
**Computation Division**  
**Huntsville, Alabama**  
**Attn: Dr. Walter P. Krause**

**Chief, Defense Atomic Support Agency**  
**Washington 25, D. C.**  
**Attn: DASAG/Library**

**U.S. Atomic Energy Commission**  
**Washington 25, D. C.**  
**Attn: Technical Reports Library**

**U.S. Atomic Energy Commission**  
**Division of Military Applications**  
**Germantown, Md.**

**Advisory Group on Elec Parts**  
**Mcore School Building**  
**200 S. 33rd St.**  
**Philadelphia 4, Pennsylvania**  
**Attn: Allan M. Hadley**

**Director**  
**Advanced Research Projects Agency**  
**Washington 25, D. C.**  
**Chief, Technical Operations Division**

**Atomic Energy Commission**  
**Space Nuclear Propulsion Office**  
**Washington 25, D. C.**  
**Attn: F. C. Schwenk**

**University of Maryland**  
**Director, Wind Tunnel**  
**College Park, Maryland**  
**Attn: Donald S. Gross**

**United Aircraft Corporation**  
**Research Division**  
**East Hartford 8, Connecticut**  
**Attn: Mr. R. Olsen**

**Los Alamos Scientific Laboratory**  
**Los Alamos, New Mexico**  
**Attn: Library**

**U.S. Library of Congress**  
**Washington 25, D. C.**  
**Attn: Science & Technology Division**

DISTRIBUTION (Cont'd)

Army Engineer Research & Development Laboratories  
Fort Belvoir, Virginia  
Attn: Chief, Mechanical Dept

University of New Mexico  
Albuquerque, New Mexico  
Attn: Dr. Richard Moore

University of Michigan  
Institute of Science & Technology  
2038 E. Engr Bldg  
Ann Arbor, Mich  
Attn: R. R. White, Director

University of Maryland  
College of Aeronautical Engineering  
College Park, Maryland  
Attn: W. Sherwood

University of Florida  
Physics Department  
Gainesville, Florida  
Attn: Technical Library - Alex G. Smith  
Attn: L. H. Roberts

Engineering Library  
University of California  
405 Hilgard Avenue  
Los Angeles 24, California  
Attn: Mrs. J. E. Tallman

Engineering Library  
University of California  
Berkeley, California  
Attn: Mrs. Blanche Dalton

University of Arizona  
Physics Department  
Tucson, Arizona  
Attn: Professor Ulrich H. Bentz

Sandia Corporation  
Sandia Base  
Albuquerque, New Mexico  
Attn: Technical Library

DISTRIBUTION (Cont'd)

Rensselaer Polytechnic Institute  
Dept of Aeronautical Engineering  
Troy, New York  
Attn: Mr. K. T. Yen

Patent Office  
Washington 25, D. C.  
Attn: Scientific Library

Ohio State University  
576 Melrose Avenue  
Columbus 2, Ohio  
Attn: Technical Library

New York Naval Shipyard  
Bldg 291, Code 912B  
Brooklyn 1, New York  
Attn: Library

National Physical Laboratory  
Teddington, Middlesex, England  
Attn: Technical Library  
Thru: AMC Detachment No. 1, Washington 25, D. C.  
Attn: ORDTN

National Bureau of Standards  
Bldg 16 - Rm 310  
Washington 25, D. C.  
Attn: Chief Section 1.06

National Bureau of Standards  
Boulder, Colorado  
Attn: Technical Library

National Bureau of Standards  
Washington 25, D. C.  
Attn: Library

Minneapolis-Honeywell Regulator Company  
2753 Fourth Avenue, S.  
Minneapolis 8, Minn.  
Attn: Mr. H. Sparrow

Massachusetts Institute of Technology  
Dept of Mechanical Engineering  
Cambridge, Mass.  
Attn: L. Shearer

Linda Hall Library  
Joseph C. Shipman  
5109 Cherry Street  
Kansas City 10, Missouri

DISTRIBUTION (Cont'd)

Johns Hopkins University  
Applied Physics Laboratory  
8621 Georgia Avenue  
Silver Spring, Maryland  
Attn: Tech Library (2 copies)

Franklin Institute of the State of Pennsylvania  
Philadelphia 3, Pennsylvania  
Attn: C. W. Hargens, Tech Director

Mr. Charles A. Belsterling  
Franklin Institute of the State of Pennsylvania  
Philadelphia 3, Pennsylvania

Engineering Societies Library  
29 W. 39th Street  
New York 18, New York  
Attn: Mr. John Herling, Order Librarian

Dayton & Montgomery County Public Library  
215 East Third Street  
Dayton 2, Ohio  
Attn: Circulation Department

Corning Glass Works  
Corning, New York  
Attn: James K. Davis

Cornell University  
Ithaca, New York  
Attn: Dr. Ed Resler, Jr.

John Crerar Library  
86 E. Randolph Street  
Chicago 1, Illinois  
Attn: H. Henkle

Battelle Memorial Institute  
Chief Systems Engr Div  
505 King Avenue  
Columbus 1, Ohio  
Attn: Chief Systems Engr. Div.

Armour Research Foundation of Illinois Ins. of Tech. Center  
10 W 45th Street  
Chicago 16, Ill  
Attn: Mr. George T. Jacobi

Distribution (Cont'd)

Commanding Officer  
U.S. Army Limited War Laboratory  
Aberdeen Proving Ground, Maryland  
Attn: Lt Col J. T. Brown

Mr. W. S. Hinman, Jr.  
Deputy Assistant Secretary of the Army  
Research & Development  
Room 3E390, The Pentagon  
Washington 25, D. C.

Office of the Director of Defense  
Research & Engineering  
Asst. Dir of Research Engineering (Defense)  
The Pentagon, Washington 25, D. C.

Institute for Defense Analysis  
Gordon Rausbeck  
Advanced Research Projects Div  
The Pentagon,  
Washington 25, D. C.

Commander  
U.S. Naval Ordnance Laboratory  
Corona, California  
Attn: Technical Library

Jet Propulsion Laboratory  
Pasadena, California  
Attn: Library

USCONARC  
Liaison Group  
The Pentagon (Rm 3E366)  
Washington 25, D. C.

Office of the Director of Defense Research & Engineering  
AMC Detachment No. 1  
Temporary Bldg 1  
Washington 25 D. C.  
Attn: Director of Weapons Systems Evaluation Group (Rm 2E812)

Commander  
U.S. Naval Ordnance Test Station  
China Lake, California  
Attn: Technical Director

Commander  
Edwards Air Force Base, Calif  
Attn: AFTTC(FTOOT)

DISTRIBUTION (Cont'd)

Internal

Horton, B.M./McEvoy, R.W., Lt Col  
Apstein, M./Gerwin, H.L./Guarino, P.A./Kalmus, H.P.  
Spates, J.E./Schwenk, C.C.  
Hardin, C.D., Lab 100  
Sommer, H., Lab 200  
Hatcher, R.D., Lab 300  
Hoff, R.S., Lab 400  
Nilson, H., Lab 500  
Flyer, I.N., Lab 600  
Campagna J.H./Apolenis, C.J., Div 700  
DeMasi, R., Div 800  
Landis, P.E./Horsey, E.F., Lab 900  
Seaton, J.W., 260  
Keller, C., 300  
Kirshner, J., 310  
Warren, R., 310  
Woodward, K., 310  
Peperone, S., 310  
Scudder, K., 310  
Moorhead, J., 310  
Campagnuolo, C.J., 310  
Carter, V., 310  
Goto, J., 310  
Gotttron, R., 310  
Hobbs, E., 310  
Holmes, A., 310  
Katz, S., 310  
Keto, J., 310  
Marsh, D., 310  
Mon, G., 310  
Palmisano, R., 310  
Straub, H., 310  
Toda, K., 310  
Ravitsky, C., 320  
Harris, F., 320  
Talkin, A., 240  
Ravillious, F., 240  
Burton, W., 240  
Technical Reports Unit, 800  
Technical Information Office, 010 (10 copies)  
DOFL Library (5 copies)  
Rotkin, I./Godfrey, T.B./Eichberg, R. L.  
Bryant, W. T./Distad, M. F./McCoskey, R. E./Moorhead, J. G.  
(2 pages of abstract cards follow.)

Garver, R., 250  
Eiseman, J., 310

AD \_\_\_\_\_ Accession No. \_\_\_\_\_

Diamond Ordnance Fuze Laboratories, Washington 25, D. C.

FLUID AMPLIFICATION—4. Gain Analysis of the Proportional Fluid Amplifier -- S. J. Peperone, Silas Katz, John M. Goto

TR-1073, 30 October 1962, 21 pp text, 18 illus, Department of the Army Proj 5N03-01-003, OMS Code 5010.11.71200, DOFL Proj 31100, UNCLASSIFIED Report

1. Pneumatic systems—Gain analysis
2. Proportional fluid amplifiers—Design concepts
3. Fluid flow—Theoretical analysis
4. Hydraulic systems—Theory
5. Gain analyses—Comparison of theoretical and experimental results

A theoretical analysis of signal gain using principles of fluid stream interaction is presented. This analysis is applied to predict pressure, flow, and power gains of a fluid amplifier and to determine optimum operating conditions and geometry. Comparison of theory and measurements show agreement within the experimental error.

AD \_\_\_\_\_ Accession No. \_\_\_\_\_

Diamond Ordnance Fuze Laboratories, Washington 25, D. C.

FLUID AMPLIFICATION—4. Gain Analysis of the Proportional Fluid Amplifier -- S. J. Peperone, Silas Katz, John M. Goto

TR-1073, 30 October 1962, 21 pp text, 18 illus, Department of the Army Proj 5N03-01-003, OMS Code 5010.11.71200, DOFL Proj 31100, UNCLASSIFIED Report

1. Pneumatic systems—Gain analysis
2. Proportional fluid amplifiers—Design concepts
3. Fluid flow—Theoretical analysis
4. Hydraulic systems—Theory
5. Gain analyses—Comparison of theoretical and experimental results

A theoretical analysis of signal gain using principles of fluid stream interaction is presented. This analysis is applied to predict pressure, flow, and power gains of a fluid amplifier and to determine optimum operating conditions and geometry. Comparison of theory and measurements show agreement within the experimental error.

AD \_\_\_\_\_ Accession No. \_\_\_\_\_

Diamond Ordnance Fuze Laboratories, Washington 25, D. C.

FLUID AMPLIFICATION—4. Gain Analysis of the Proportional Fluid Amplifier -- S. J. Peperone, Silas Katz, John M. Goto

TR-1073, 30 October 1962, 21 pp text, 18 illus, Department of the Army Proj 5N03-01-003, OMS Code 5010.11.71200, DOFL Proj 31100, UNCLASSIFIED Report

1. Pneumatic systems—Gain analysis
2. Proportional fluid amplifiers—Design concepts
3. Fluid flow—Theoretical analysis
4. Hydraulic systems—Theory
5. Gain analyses—Comparison of theoretical and experimental results

A theoretical analysis of signal gain using principles of fluid stream interaction is presented. This analysis is applied to predict pressure, flow, and power gains of a fluid amplifier and to determine optimum operating conditions and geometry. Comparison of theory and measurements show agreement within the experimental error.

AD \_\_\_\_\_ Accession No. \_\_\_\_\_

Diamond Ordnance Fuze Laboratories, Washington 25, D. C.

FLUID AMPLIFICATION—4. Gain Analysis of the Proportional Fluid Amplifier -- S. J. Peperone, Silas Katz, John M. Goto

TR-1073, 30 October 1962, 21 pp text, 18 illus, Department of the Army Proj 5N03-01-003, OMS Code 5010.11.71200, DOFL Proj 31100, UNCLASSIFIED Report

1. Pneumatic systems—Gain analysis
2. Proportional fluid amplifiers—Design concepts
3. Fluid flow—Theoretical analysis
4. Hydraulic systems—Theory
5. Gain analyses—Comparison of theoretical and experimental results

A theoretical analysis of signal gain using principles of fluid stream interaction is presented. This analysis is applied to predict pressure, flow, and power gains of a fluid amplifier and to determine optimum operating conditions and geometry. Comparison of theory and measurements show agreement within the experimental error.

REMOVAL OF EACH CARD WILL BE NOTED ON INSIDE BACK COVER, AND REMOVED CARDS WILL BE TREATED AS REQUIRED BY THEIR SECURITY CLASSIFICATION.